ASM Handbook, Volume 11, *Failure Analysis and Prevention*
B. Miller, R. Shipley, R. Parrington, D. Dennies, editors
DOI 10.31399/asm.hb.v11.a0006791

Adhesive Wear Failures

Bojan Podgornik, Institute of Metals and Technology

FRICTION AND WEAR are important when considering the operation and efficiency of components and mechanical systems. The friction between contact surfaces in motion results in wasted energy and generated heat, whereas any type of wear can lead to a degradation in surface quality, unexpected clearances, a loss of material and efficiency, and finally component failure (Ref 1).

Among the different types and mechanisms of wear, adhesive wear is very serious. It is characterized by high wear rates and a large, unstable coefficient of friction. Sliding contacts can be rapidly destroyed by adhesive wear; in extreme cases, sliding motion can be prevented by a very high coefficient of friction or a combination of material transfer and adhesion. Metals and alloys are particularly prone to adhesive wear, with the majority of adhesive wear failures being related to the breakdown of the lubrication film in the sliding contacts. Lubrication (or other forms of protective-surface film) breakdown relates to the loss of the basic function of the protective film—to provide some degree of separation between the sliding surfaces. If the sliding surfaces are not separated, then adhesion and subsequent wear are almost inevitable (Ref 2).

The well-investigated tendency of all materials to mutually adhere when brought into close contact is the basic cause of adhesive wear. Although contaminants, protective-surface films, and lubricants provide effective means of preventing adhesive wear, they can never entirely eliminate it. Adhesion results in a high coefficient of friction as well as in serious damage to the contacting surfaces. In extreme cases, it may lead to complete prevention of sliding; as such, adhesive wear represents one of the fundamental causes of failure for most metal sliding contacts, accounting for approximately 70% of typical component failures (Ref 2).

Mechanism of Adhesive Wear

Adhesive wear is characterized by the transfer of a material from one contacting surface to another during the relative motion caused by localized bonding. It occurs when high loads, temperatures, or pressures cause the asperities on two contacting metal surfaces in relative motion to deform and spot weld together, followed by plowing, tangential shearing, and tearing of the metal in small, discrete areas called microjoints (Ref 3, 4). The engineering terms used to describe adhesive wear include *seizing*, *galling*, *scoring*, and *scuffing*. Adhesive wear occurs because the adhesive bond is stronger than the cohesive bond within the weaker material of the contact pair (Ref 5). Even though a contact surface may seem smooth, it actually consists of many valleys and asperities, so-called "high spots." The load applied to the contact surfaces will be transferred through these high spots, causing very high local pressures and thus increasing the risk of metal-to-metal contact (Ref 6), leading to adhesive wear. As sliding continues, new junctions are formed, while the transferred fragments can be transferred back to the original surface or form loose wear particles (Ref 7).

Adhesive wear is heavily dependent on the mutual affinity between the materials and is very common in metals, taking place in poor lubricating conditions or when materials slide against each other without any lubrication (Ref 8). Normally, adhesion occurs when two chemically similar metals are in contact or the contact surfaces are free from oxide layers (Ref 5). The small addition of alloying elements in the bulk material can alter the adhesion between the surfaces. In the case of dissimilar metals, when mutually insoluble metals come into contact with each other, they generally exhibit poor adhesion (Ref 9). However, in this case, if the surfaces are atomically clean, the adhesion would also be strong. Regardless of the solubility, the hardness and ductility of the material also play important roles. Softer metals exhibit larger real contact areas, which are responsible for the stronger adhesion (Ref 10). It also appears that ductility has the undesirable effect of accentuating adhesive wear (Ref 11).

The strong adhesion observed between metals can be explained by the electron transfer between contacting surfaces. Numerous free electrons are present in metals, and on contact, electrons can be exchanged between the two solids to establish bonds. The electrons are not bound by a rigid structure, and, provided that the distance between the two bodies in contact is sufficiently small (<1 nm), they can move from one body to another, resulting in bonds between two solids, despite their differing atomic structures (Ref 2, 12). All metals show a strong tendency to adhere on contact with another solid, but there are significant differences between particular elements. It has been found experimentally that metals with a hexagonal close-packed structure show much less adhesion than other crystal structures. A high hardness, a large elastic modulus, and a low surface energy also suppress the adhesion of the metal (Ref 13, 14). The reason for the difference in adhesion between metals of similar hardness but different crystal structures is believed to lie in the necessity for some degree of plastic deformation between asperities before a true contact can be established (Ref 2). Hexagonal close-packed metals have far fewer slip systems and are therefore less ductile than face-centered and body-centered metals, which results in their lower adhesion. The adhesion between metals is also influenced by the chemical reactivity or electropositivity of the individual metals (Ref 13). Chemically active metals such as aluminum bond more readily and therefore show stronger adhesion than noble metals. This suggests that a face-centered cubic metal with a high level of chemical activity would show very strong adhesion (Ref 2).

During the adhesion process and material transfer, particles are removed from one contact surface and either permanently or temporarily attached to the other surface by a cold welding process, thus leaving pits, voids, or cavities on the surface (Ref 5) and causing roughening of both contact surfaces as well as rapid wear (Ref 1). Due to the cold welding process, the generated particles are harder than the surfaces from which they originate and thus can cause great damage and speed up abrasive and erosive wear (Ref 6). As such, adhesive wear initiates microscopically but progresses macroscopically.

The adhesive wear failure process can be summarized as (Ref 15, 16) (Fig. 1):

1. Formation of adhesive microjunctions
2. Deformation of contacting asperities

3. Removal of protective oxide surface films
4. Crack initiation and propagation
5. Failure of junctions by shearing and tearing, and transfer of material

Shearing and tearing take place either at the cold-welded junction or inside the original materials, depending on which is weaker. If the strength of the adhesive junction is relatively low, as is the case for contact pairs with a low mutual solubility or metallic surfaces that are separated by an oxide or some sort of protective boundary film, tearing will take place at the junction, and the surface damage and material loss during wear will be minimal. However, when tearing occurs inside the material—and as shown by numerous investigations on a wide variety of metal combinations, this will happen within the softer or weaker material (Ref 2)—a fragment of the softer material will be dragged away and adhered to the counterbody, which is referred to as material transfer (Ref 17) (Fig. 2), a characteristic feature of adhesive wear. This can lead to an enormous increase in wear rate (Ref 15). In such cases, a large frictional force and plastic deformation caused by dislocations are introduced to the contact region. As a result of such a large deformation, a crack is initiated and is propagated in the combined fracture mode of tensile load and shearing. Material in the weaker asperity deforms in a series of shear bands to accommodate the relative movement, and when the shear band reaches a certain limit, a crack is initiated or an existing crack progresses until a new shear band is formed (Fig. 3). When the crack reaches the contact interface, a wear particle is formed, and material transfer is completed (Ref 16).

Adhesive material transfer can be in the form of either thin flakelike or wedgelike wear particles, as described by Kayaba and Kato in Ref 18. Tangential shear under compression at the contact interface of a strong adhesive bond generates slips along the slip planes in the contact region. As a result of the slips, flakelike shear tongues are formed, as shown in Fig. 4(a), followed by crack initiation and propagation in the combined fracture mode of the tensile load and shear in the leading region of the contact. The large plastic deformation in the contact region sometimes forms a wedgelike shape, which is followed by crack initiation and propagation in the combined fracture mode of the tensile load and shear in the trailing region of the contact, as shown in Fig. 4(b). In the process of adhesive wear, transfer and retransfer from one surface to the mating surface can also take place. As a result, relatively large lamella-type adhered wear particles composed of two surfaces are formed (Ref 19). In the successive process of repeated sliding, these wear particles can leave the contact interface as free particles or stay adhered, forming prows to scratch the countersurface and prevent smooth sliding (Ref 20, 21).

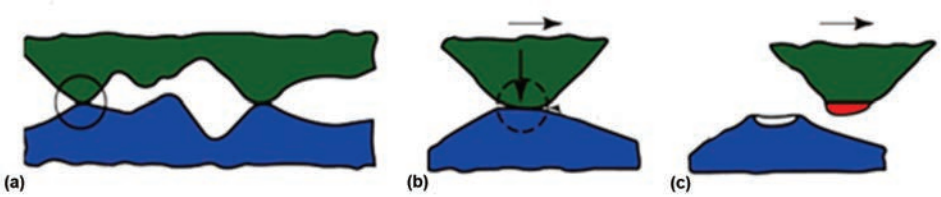

Fig. 1 Steps leading to adhesive wear. (a) Microjoints. (b) Deformation of asperities and removal of surface films. (c) Shearing and material transfer. Source: Ref 15

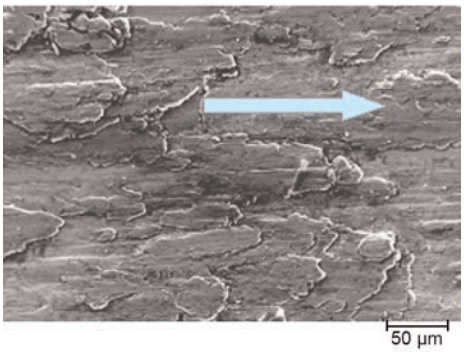

Fig. 2 Example of adhesive wear characterized by excessive material transfer, shown by transferred layers of titanium alloy on a steel surface. Source: Ref 17

As mentioned, the wear particles generated as a result of adhesive wear and material transfer can detach from the contact surfaces and become third-body abrasive particles, resulting in intensified erosive and abrasive wear. Experimental results have even shown a much higher probability of wear-particle generation due to asperity contacts during adhesive wear compared to, for example, abrasive wear (Ref 22). A possible mechanism for third-body particle formation in an adhesive sliding contact has been discussed using a two-dimensional coarse-grained numerical simulation (Ref 23). These simulations revealed the existence of a critical length scale that controls the formation of the particles during the adhesive interaction between surface asperities. Only asperity junctions larger than the critical length scale form loose particles or debris, while the smaller ones are smoothed out plastically. The critical junction size model (Ref 24) predicts the transition between two adhesive wear mechanisms: gradual plastic shearing versus fracture-induced particle formation. As two asperities approach, a strong adhesive bond is established between them, leading to a buildup of stored elastic energy in the junction (Fig. 5a) caused by the deformation of asperities. Upon sliding, two mechanisms for junction failure can be described: the adhesive junction fails by severe plastic deformation (Fig. 5b), or cracks form and propagate at the base of the asperities, eventually reaching the surfaces, which results in third-body wear-particle formation (Fig. 5c). The critical junction size

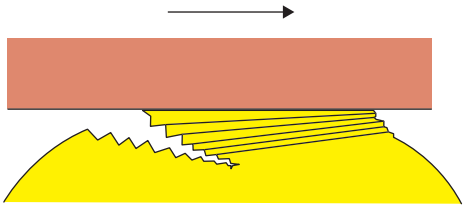

Fig. 3 Crack initiation and propagation at a microjunction. Adapted from Ref 16

model predicts debris formation in the case of metals for junction sizes above tens of micrometers, while gradual plastic failure can be observed for asperities up to 60 nm (Ref 25). For mild adhesive wear, the particles formed will often be in the form of oxide flakes on the order of 0.01 to 1.0 μm; for severe adhesive wear, the particles are metallic and more chunky, on the order of 10 to 100 μm (Ref 1).

The wear volume of the particles generated by adhesive wear (W) under normal load (F_N) after sliding for a certain distance (L) is given by (Ref 16):

$$W = \frac{1}{3} \cdot \frac{F_N \cdot L}{H} \qquad \text{(Eq 1)}$$

The adhesive wear volume is proportional to the normal load and the sliding distance and is inversely proportional to the hardness (H) of the wearing material. It is also proportional to the total real contact area during sliding. However, adhesive wear can occur in various modes (Ref 18); wear particles are not always generated only from the softer material but can come from both materials, and the size of the wear particles does not simply correspond to the size of the contact. The probability of wear-particle generation at each contact point is also not equal; it depends on the microscopic shape of the contact, the microstructure of the material in the contact region, the microscopic surface contamination, and the surrounding environment (Ref 16). To accommodate all these variables, a parameter K_{ad} (the adhesive wear coefficient), varying between 10^{-7} and 10^{-2} and being dependent on the operating conditions and material properties, is introduced into Eq 1 as a modifier. The wear volume is then described as:

$$W = K_{ad} \cdot \frac{F_N \cdot L}{H} \qquad \text{(Eq 2)}$$

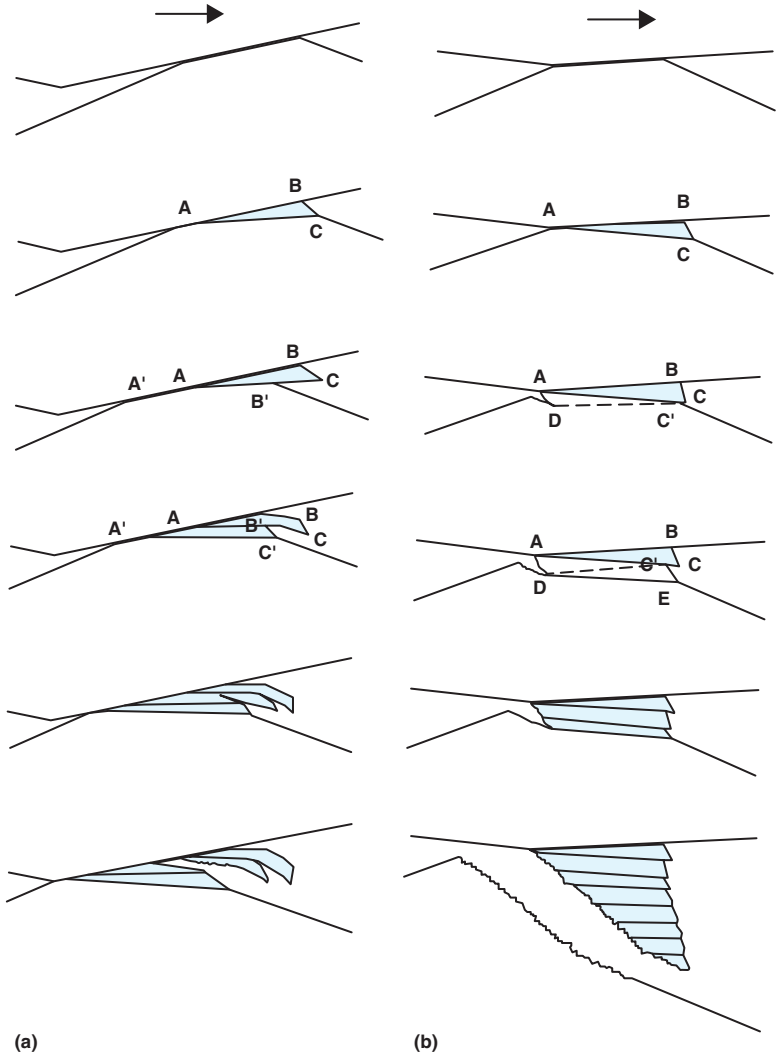

Fig. 4 Schematic diagram of the adhesive transfer process of (a) a thin, flakelike wear particle and (b) a wedgelike wear particle. Numbers indicate generation of slips along the slip planes (how certain "adhesive bond" moves along the contact). First bond is indicated by numbers and the next one with primes. Adapted from Ref 18

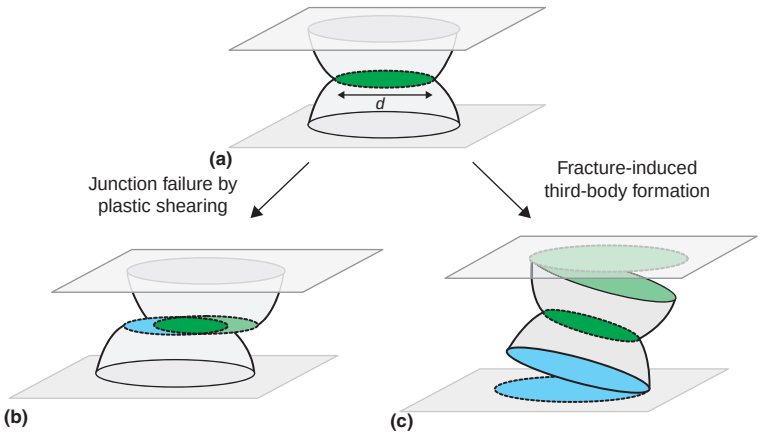

Fig. 5 Adhesive wear mechanisms. (a) Adhesive bonding. (b) Plastic shearing. (c) Fracture-induced formation of third-body particles. Adapted from Ref 25

The adhesive wear coefficient, K_{ad}, is the principal value for a friction pair describing its wear rate. The physical meaning of K_{ad} is the wear volume fraction in the plastic contact zone, and it is strongly affected by the material properties and the geometry of the zone during compression and shearing (Ref 16).

Adhesive Wear Failure Modes

Besides during dry sliding, adhesive wear occurs in applications and contacts operating in the mixed- and boundary-lubrication regimes, due to insufficient lubrication supply, inadequate viscosity, incorrect internal clearances, incorrect installation, or misalignment. Adhesive wear also can cause rapid and sometimes catastrophic failures (Ref 2). This can occur in metal forming, piston rings, skirts and cylinders, chains, cams and follower bearings, and gears (Ref 26). The normal break-in is a form of mild adhesive wear.

Scuffing usually refers to moderate adhesive wear, while galling, smearing, seizing, and scoring result from severe adhesion (Ref 4). When material is transferred from one counterbody (normally the softer one) to another, the effect is called scuffing, scoring, or galling. However, when a considerable area of the rubbing surfaces is joined as a result of the friction, it is described as seizure or smearing of one of the bodies by the counterbody (Ref 3).

The main factors affecting the severity of adhesive wear as well as its mode or type include (Ref 27):

- Components and tool design
- Applied load
- Contact area and degree of movement
- Lubricant type and lubrication mode
- Environment
- Material properties (i.e., surface finish, hardness, microstructure)

To reduce the risk of adhesive wear or limit it to low severity, the contact load on the sliding surfaces should be kept low, while the contact area should be maximized. In these low-contact-pressure situations, lubrication (especially its viscosity) (Ref 28) plays an important role, and the design must ensure that adequate lubrication can be effectively delivered to the components in relative motion and prevent direct metal-to-metal contact. On the other hand, the surface finish of contact surfaces is very important, because highly polished (R_a < 0.25 μm) or very rough (R_a > 1.5 μm) surfaces increase the tendency for adhesion and material transfer. Smooth surfaces result in more contact and increased adhesive forces. The absence or very small dimensions of the valleys and asperities on a smooth surface mean that the lubricant cannot be held in place between the surfaces, and any generated wear particles are retained in close contact with the surfaces, resulting in

wear. Rough surfaces result in the interlocking of asperities, which promotes severe tearing and adhesive wear in different forms. Also, the hardness and microstructure of the material play an important role in adhesive wear. A high hardness (obtained by work hardening or heat and surface treatment), a stable oxide film on the contact surface, and material with a low surface shear resistance can provide improved resistance to adhesion (Ref 27).

Scoring

Scoring is defined as a severe form of adhesive wear that appears as severe and extensive scratches and grooves in the direction of sliding. It is typical for contacts with substantial sliding between the lubricated surfaces. Scoring is a gradual process and the combined result of two distinct activities (Ref 29, 30): lubrication failure in the contact region, and the establishment of metal-to-metal contact. Scoring occurs due to the tearing out of small particles that weld together (as a result of sliding forces), overheating (due to high contact pressure and/or high sliding speed), and metal-to-metal contact (Ref 15). The cold welding and tearing action remove the transferred metal rapidly and continuously, so long as the load, speed, and lubricant temperature remain at the same level. Scoring can be classified into initial, moderate, and destructive forms (Ref 30).

Initial scoring occurs at the ridges and protrusions left by forming and machining operations. Gradual breakdown and lubrication failure at these spots lead to initial scoring. It is characterized by the appearance of fine scratches on the rubbing surfaces, often accompanied by the formation of transverse cracks, particularly on the slower surface (Ref 29). Once the high spots are smoothed out or removed, the contact stress decreases as the load is distributed over a larger area. Scoring will then stop if the load, speed, and lubricant temperature remain unchanged or if they are reduced. Initial scoring is nonprogressive and can be suppressed or even eliminated. If the load, speed, or lubricant temperature is increased, scoring will spread over a larger area, resulting in moderate scoring, which progresses at a reasonable rate. The material begins to transfer, mainly from the slower to the faster surface, and the coefficient of friction can rise to approximately 0.1 (Ref 29). However, if there is a substantial increase in load, speed, or lubricant temperature, then severe scoring will set in, with large material-transfer regions spreading quickly throughout the contact.

Sometimes scoring is also referred to as scuffing, with the terms very frequently being interchanged (Ref 15, 31). However, they are two distinct but related barriers that can limit the performance of heavily loaded sliding components lubricated by liquids. Scoring involves gross adhesive transfer, while scuffing is more involved with local plastic deformation. They both represent the final stages in lubrication breakdown and are barriers to expanding the limits of lubrication for many types of mechanical components (Ref 29).

Scuffing

Scuffing, being typical in gear applications, is a sudden and irreversible process defined as the localized damage caused by the occurrence of solid-phase welding between sliding surfaces (Ref 32–34). It is classified as a catastrophic surface failure, mainly caused by extreme local surface temperatures that are dictated by the contact pressure and sliding speed (Ref 35). Typical for scuffing is the material transfer between sliding surfaces, with parts of the surfaces becoming rough and heavily distorted (Fig. 6), thus losing their integrity and functionality (Ref 36). The original grinding marks are completely obliterated (Ref 29). It occurs nonuniformly, meaning it can start at one place on a surface and spread to another after continued operation (Ref 38). Furthermore, scuffing can result in a sudden increase in noise and vibration (overheating) as well as in a coefficient of friction rise by a factor of 2 to 4 (Ref 29), thereby further accelerating the adhesion process (Ref 39). Generally, these conditions occur in inadequately lubricated contacts (Ref 40) in which an insufficient lubrication-film thickness permits metal-to-metal contact between the contacting surfaces. Without lubrication, a direct-metal contact removes the protective oxide layer from the surface, and the excessive heat generated by the friction welds the surfaces at the contact points. As the surfaces separate, the metal is torn and transferred between the surfaces. For this reason, scuffing involves various damage mechanisms, such as mechanical, chemical, metallurgical, and thermal reactions (Ref 26). Scuffing is most likely to occur in newly machined surfaces during the running-in period, because there is insufficient operating time to smooth the contacting surfaces (Ref 31). Progressive solid-state welding and increased interfacial friction can lead to stopping the relative motion, which is known as seizure (Ref 15).

The onset of scuffing is closely related to the surface local temperature, which is the sum of the surface bulk temperature and the instantaneous temperature rise (flash temperature), caused by the local frictional heat flux. Under full-film lubrication conditions, rough surface contacts can experience high hydrodynamic pressure spikes due to surface irregularities. The pressure spikes become even more severe when the lubrication condition is the mixed elastohydrodynamic (EHD) type, where the fluid film vanishes locally and instantaneous asperity contacts take place. The sliding action between the mating surfaces generates frictional heat that increases the surface bulk temperature when the heat cannot be effectively removed through lubrication. The instantaneous flash temperature along the contact adds to the elevated bulk temperature to result in an instantaneous local surface-temperature distribution whose maximum can be above a certain critical value, affecting the viscosity and thickness of the lubrication film (Ref 41). In addition, shear stress also plays a role in determining film thickness, with a lubricant only being able to withstand a limited shear stress (Ref 42). In such a case, the outcome is scuffing in the form of solid welding and tearing of the contact surfaces (Ref 35). Therefore, lubricant viscosity and surface roughness and morphology (Ref 32) can be regarded as the main factors influencing scuffing (Ref 28). In this respect, the main design guideline is that the fluid-film thickness controlled by viscosity, load, and sliding speed must be equal to or greater than the composite surface roughness of the sliding surfaces (Ref 43). The other factors contributing to scuffing failure include wear or fatigue debris in the lubricant, wearout of the protective tribological film, lubricant degradation, and so on (Ref 44, 45).

The typical appearance of scuffed gear teeth includes the smooth, "as-machined" surfaces of the teeth being completely disrupted and

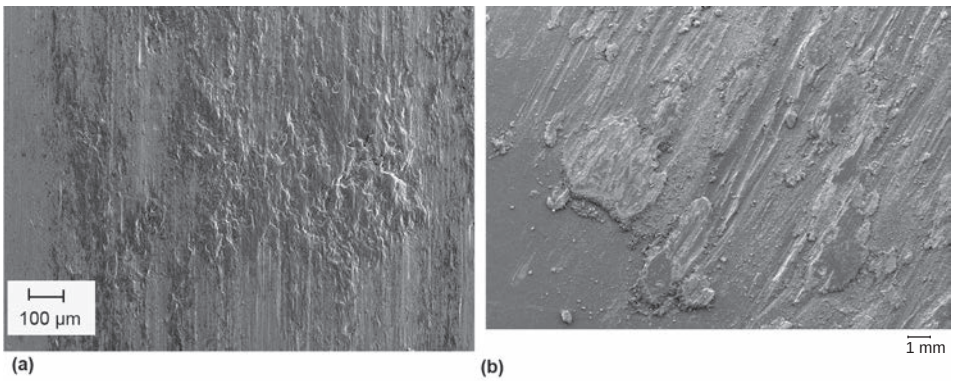

Fig. 6 Closeup of scuffing wear failure. (a) Roughening of the surface. Reprinted from Ref 37 with permission from Elsevier. (b) Material transfer. Source: Ref 38

displaying signs of strong adhesion and adhesive fracture (Ref 2).

Because scuffing resistance varies from material to material and even for samples of the same material with different thermomechanical or surface-preparation histories (Ref 46), it is important to also consider how (besides lubrication-film breakdown) mechanisms operating within the materials affect the initiation of scuffing. Hershberger et al. (Ref 39, 47) presented experimental evidence linking the initiation of scuffing to rapid plastic deformation in the near-surface material of sliding surfaces. In sliding metal contacts, plastic deformation near the surface results in work hardening, while much of the work of friction is converted into heat and a local temperature increase. These high temperatures can result in local thermal softening. If a rising contact severity (increased combination of contact pressure and sliding speed) causes the rate of thermal softening to exceed the rate of work hardening, the plastic deformation can become unstable, forming an adiabatic shear instability (Ref 39). The observations of Hershberger et al. (Ref 39) that show severe deformation of a layer of material occurring over a time frame on the order of microseconds are consistent with adiabatic shear plastic instability, which can be taken as an additional initiation mechanism for scuffing. Also, the process of shear instability can be divided into the initiation and propagation stages, each with different driving forces (Ref 36).

During the initial stage, some deformation of the near-surface material will occur as the severity of the contact increases. Initially, elastic deformation is dominant, especially under relatively mild contact and full-film EHD lubrication conditions. As contact severity and surface interaction increase, local plastic deformation will eventually occur, starting at the highest asperities. This initial plastic deformation is homogeneous, stable, and accompanied by work hardening. With further increases in contact severity, more local plastic deformation and work hardening will occur, and some of the work of plastic deformation will be converted into heat within the area of local plastic deformation. The resulting local heating produces some thermal softening of the locally deforming material. Initially, the rate of work hardening dominates. However, at some critical plastic deformation point, the rate of thermal softening will exceed the rate of work hardening, resulting in a sudden burst of dislocation motion and unstable plastic deformation. This sudden rapid deformation is the initiation of scuffing (Ref 36). Once initiated by an adiabatic shear instability with concomitant heat generation, the propagation of scuffing is governed by the competition between heat generation by more plastic deformation and heat dissipation away from the locally deformed area. If the rate of heat generation from plastic deformation is greater than the rate of heat dissipation, more thermally driven severe and unstable plastic deformation will occur, resulting in scuffing propagation; otherwise, scuffing will be limited to only the severely deformed initiation site (Ref 36).

Seizure

Seizure means to bind or fasten together; it is a result of the mutual plastic deformation of materials in contact, and it is an extreme form of adhesive wear. In ordinary cases, components do not become separated on their own after seizure; manual force is required to separate the parts (Ref 15). An example of the seizure of rolling elements is shown in Fig. 7 and of a piston in Fig. 8. The causes of seizure, which is mainly governed by excessive loading and heating, include (Ref 15):

- Poor heat dissipation, mainly related to material properties, such as thermal conductivity
- Poor lubrication system or improper lubrication
- Excessive load
- Smaller clearances caused by improper design
- Installation errors and poor/improper maintenance
- Adhesive properties of the contacting surfaces; the ability of a material to seize or to join in the solid state

Galling

Galling is an adhesive wear failure associated with forming and the tendency of a lubricant film to break down, resulting in the transfer and pickup of sheet or work material by the tool surface and subsequent macroscopic damage or even severe scratching (scoring) of the workpiece surface (Ref 50). According to the ASTM International standard G 40, galling is defined as "a form of surface damage arising between sliding solids, distinguished by macroscopic, usually localized, roughening and creations of protrusion rising above the original surface. It often includes material transfer, or plastic flow, or both." Thus, the wear in metal forming, being also the dominant cause of tool failure (Ref 51) (especially in deep drawing, fine blanking, and sheet metal forming), is often related to galling (Ref 52–54). This wear failure mode eventually results in high friction, geometric deviation, and fracture of the formed products, or worse, jamming of the tooling (Ref 50). It is a gradual process, initiated by the microscale local transfer of work material to the tool surface, which is also termed incipient galling (Ref 55). Successive forming operations lead to the formation of patches or lumps of adhered material on the metal-forming tool surface (Ref 56) (Fig. 9) and to the growth of the transfer layer (Fig. 10). During adhesion, the transferred work material can experience several hardening mechanisms (Ref 59), thus damaging the subsequently formed part by scratching and indentation and leading to unstable friction (Ref 60, 61). If the forming proceeds, tool wear is governed by severe adhesive wear with gross surface damage and high friction (Ref 52). In many cases, the

Fig. 7 Examples of the seizure of roller-bearing elements. Source: Ref 15, 48

Fig. 8 Example of seizure on a piston due to insufficient cooling. Source: Ref 49

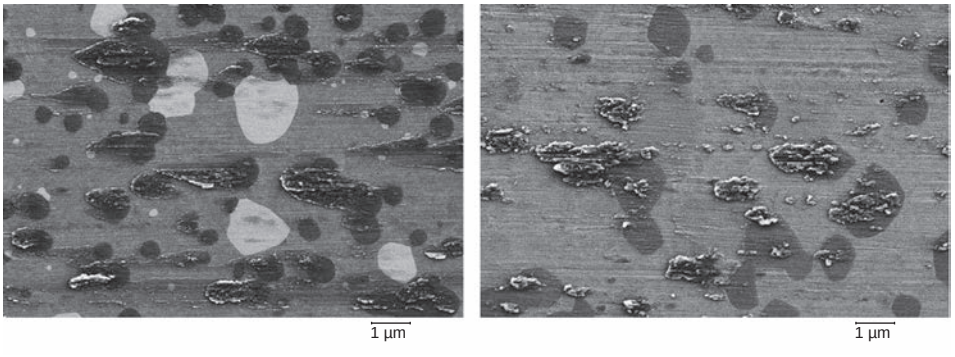

Fig. 9 Initial galling failure on powder metallurgy tool steels. Reprinted from Ref 57 with permission from Elsevier

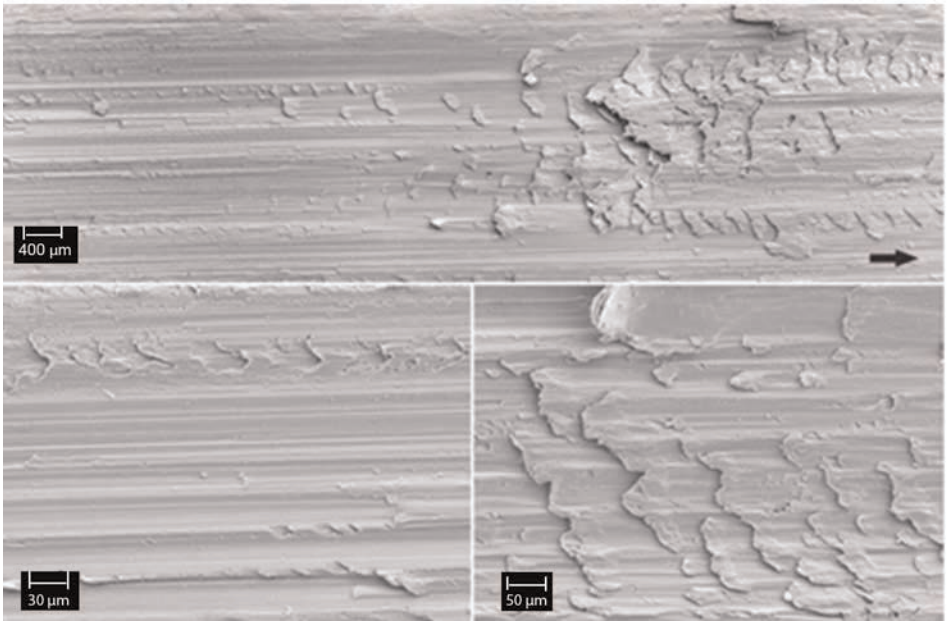

Fig. 10 Surface damage typical of galling wear on high-strength steel sheet material. Source: Ref 58

galling acts in combination with abrasive wear damage, leading to blunting of the cutting edges, which results in an increase in forming and cutting forces and consequently to accelerated tool damage (Ref 62). Various investigations into galling also showed that wear-damage features precede the galling progress through a number of stages, including asperity smoothing and plastic deformation, abrasive damage on various scales, and finally progressing to galling damage (Ref 58, 63, 64).

The tendency for galling is a limiting factor in many tribosystems (Ref 55). As a severe form of adhesive wear, the galling of tools is a frequent and major problem, not only adversely affecting the surface quality of produced parts (Ref 65) but also increasing the downtime for maintenance of tools (Ref 66). It results in local spots of material rising up from a surface, which impedes sliding against another surface. The feature of galling that sets it apart from other forms of adhesive wear is the severity and size of the protrusions from the original surface that form during the sliding process. Another common characteristic of galling is that it can occur over the course of an individual pass of one surface over another (Ref 55), resulting in varying levels of galling wear severity on a single part. Multiple galling wear sites can also be expected with the large contact areas seen in deep drawing (Ref 65). However, although it occurs very frequently, galling is still not thoroughly understood, with different initiation mechanisms being proposed related to adhesion, surface defects, microstructure, efficiency of lubrication, and temperature (Ref 64).

It has been shown that galling is influenced by factors such as tool and sheet microstructure and mechanical properties, surface roughness, type of lubricant, and contact conditions (Ref 67). Materials that are highly ductile or which possess low work-hardening rates are known to be prone to galling (Ref 27). However, in metal forming, the surface roughness of the tool has been found to be the most important factor influencing galling initiation (Ref 61, 66, 68, 69). Beyond the commonly considered surface-roughness parameters, such as R_a or R_z, the ratio of peaks to valleys (R_{pk}/R_{vk}) as well as the skewness and kurtosis (R_{sk}, R_k) of the surface were identified as significantly influencing the galling kinetics (Ref 51, 62). Furthermore, numerous investigations (Ref 68, 70) have shown that galling tends to initiate at irregularities on the surface and that it cannot be completely avoided; only the growth rate of the transferred layer can be controlled (Ref 68, 71). Initial galling was found to happen in a directional manner, in the form of material accumulations in front of microscopic surface asperities (Ref 62), which then progresses toward moderate, heavy, and severe galling, as shown in Fig. 11. The tendency for galling to occur can be reduced by using dissimilar and harder materials of low ductility, lubrication, and surface smoothing (Ref 73). Furthermore, the formation of glaze layers through oxidized wear debris as well as the use of surface-engineering techniques were

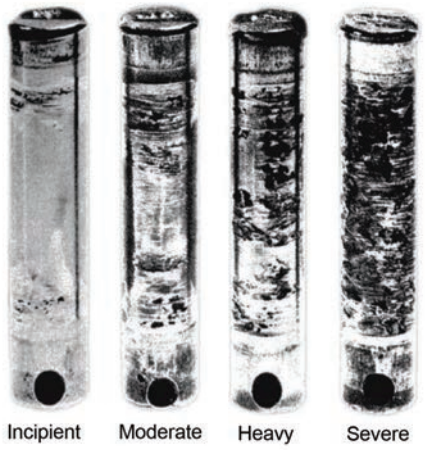

Fig. 11 Intensity of galling, ranging from incipient to moderate, heavy, and severe. Source: Ref 72

found to significantly reduce the occurrence of galling (Ref 66).

Testing and Evaluation of Adhesive Wear

The experimental research and evaluation of adhesive wear failures should include classic laboratory-type and standardized tests, in which each influencing parameter can be isolated, controlled, and monitored, as well as technological modeling tests conducted to allow the transferability of the results to industry and real-world applications (Ref 74).

Standardized Galling Tests

Over the years, several test methods have been developed to measure and evaluate the resistance of materials to adhesive wear, especially its most severe form, known as galling. The most widely used galling test, first approved in the 1980s, is ASTM International G 98-02, "Standard Test Method for Galling Resistance of Materials" (reapproved in 2009), often referred to as the "button-on-block test." This method does not require dedicated wear-test equipment to run the test; it only requires a relatively common universal testing machine that can exert a constant compressive force or load between the mating specimens. The ASTM International G 98 test method was presented by Schumacher of Armco Steel Corporation in the early 1970s and has been used since that time to determine the relative galling resistance of one material pair versus another (Ref 75). ASTM International G 98 is strictly a qualitative method, as outlined in ASTM International G 98, 5.5: "This test method should not be used for quantitative or final design purposes." However, the standard does report a threshold galling stress that has been used as a ranking value to screen materials and material pairs in terms of their galling resistance (Ref 76).

In the case of ASTM International G 98, a constant load is placed on the button, which is then rotated one revolution (360°) relative to the stationary block (Fig. 12a). Upon completion of the test, the specimens are examined visually for the presence of galling (Fig. 13). If galling has not occurred, then new specimens are loaded at a higher level and tested. This is continued until galling occurs, at which point the load of the highest nongalled test is averaged with the load of the lowest galled test. This load is divided by the cross-sectional area of the button specimen and is deemed the threshold galling stress. A major drawback of the ASTM International button-on-block test is its lack of precision; the threshold galling stress measured can vary by a factor of 4 or more (Ref 75). One of the contributing factors to the low precision is the subjective determination of the presence of galling, with the

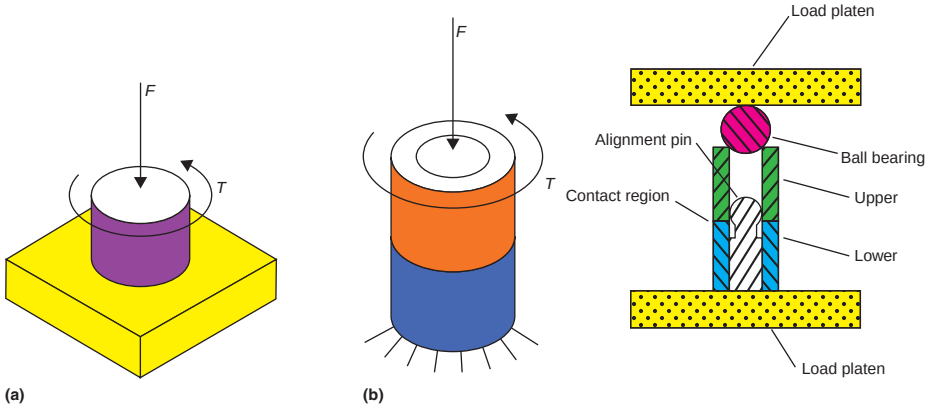

Fig. 12 (a) Original ASTM International G 98 button-on-block test configuration. *F*, force; *T*, torque. Adapted from Ref 77. (b) Modified cylinder-on-cylinder ASTM International G 196 test configuration. Adapted from Ref 75

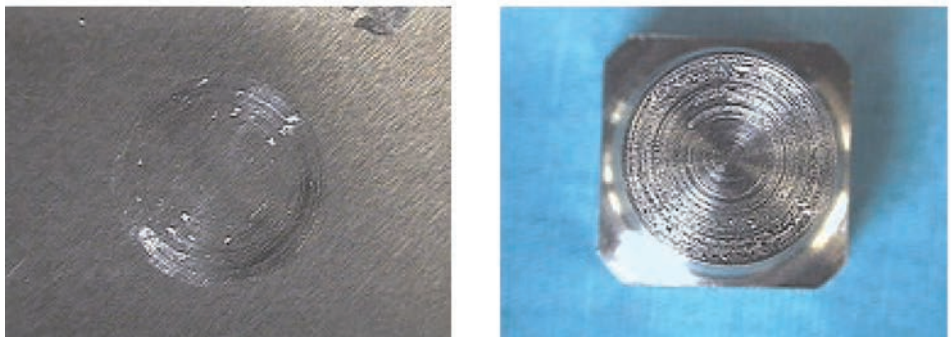

Fig. 13 Examples of typical wear scar for ASTM International G 98 test. Courtesy of K.G. Budinski, Bud Labs

standard only defining states as either "galled" or "not galled." However, for wear-resistant materials, damage can progress through a range of behaviors (Ref 78) and also require a definition of the galling severity. Another factor is the stress concentrations at the button edge, as well as the stochastic nature and probability of the galling process (Ref 75). As included in ASTM International G 196, the threshold galling stress specified in ASTM International G 98 can be replaced with a "$Galling_{50}$" value, defined as the stress at which 50% of the specimens are expected to gall.

Clearly, it is almost impossible to achieve repeatable results and collect a quantifiable output on galling and galling severity by using only visual assessments (Ref 79). In an effort to remove the subjectivity of a visual assessment of galling, a friction-based criterion (Ref 80) can be used to define galling based on the critical friction level and/or by employing a surface-topography technique to analyze the surface finish before and after testing (Ref 81). A numerical ranking of galling severity has been proposed and used to provide a quantitative output for visual assessment (Ref 55, 63, 82). However, in these instances, the assessment is made on magnified regions with a consistent and more-or-less uniform wear state. Such an approach is less suitable for industrial-style experiments because it is difficult to apply to larger contact regions with multiple localized instances of adhesive wear. It is evident that all adhesive wear failures, including galling, share the characteristic of sudden changes in height above and below the level of the bulk material. This characteristic can be well captured by a surface-topography analysis perpendicular to the sliding direction and may be used for possible galling wear identification and quantification. A methodology allowing the measurement and quantification of galling wear severity is based on the discrete wavelet transform of two-dimensional surface profiles (Ref 79). The localized wavelet functions that are used in the wavelet transform are ideal for detecting wear features and correlate well with the shape of galling features, such that it is possible to separate galling from surface roughness and quantify its severity.

To address the problem of stress concentrations, Hummel (Ref 83) developed a test method with line contact, obtained by pairing a stationary button with a rotating cylinder. On the other hand, a new test geometry

(Fig. 12b) was presented by Budinski et al. (Ref 84) that eliminates the stress concentration present at the outside diameter of the button in the ASTM International G 98 test. It also addresses problems with zero sliding distance, which is present at the center of the button in the original ASTM International G 98 button-on-block test. A modified test configuration standardized under the ASTM International G 196 test uses two concentric hollow cylinders (Fig. 12b) of the same outer diameter as the button in the ASTM International G 98 test, forming the contact area in the shape of an annulus. To achieve proper alignment of the specimens, an alignment pin is used, consisting of a cylindrical lower region with a spherical upper region. To conduct the test, the bottom specimen is fixed while a load (F) is applied to the upper specimen, which is rotated via an applied torque (T). Analogous to the standard test, the specimens are examined for the presence of galling upon completion of the test. However, another difference between ASTM International G 98 and G 196 is that the latter uses the $Galling_{50}$ stress metric, with the probability of galling occurring on one or both test specimens being 50%. At least four test forces are required, and at least 12 replicates are tested at each force (Ref 55).

Classic Laboratory-Type Tests

In addition to standard galling tests, several different test methods have been developed to analyze wear resistance and study wear failures, including ASTM International G 77, "Standard Test Method for Ranking the Resistance of Materials to Sliding Wear Using Block-on-Ring Wear Test," and ASTM International G 99, "Standard Test Method for Wear Testing with a Pin-on-Disk Apparatus." However, much of the published data on adhesive wear and adhesive wear resistance is generated based on a simple pin-on-disk test employing a spherical-tipped pin-and-point contact (Fig. 14a) (Ref 85–88); another one is the cylinder-on-cylinder test (Fig. 14b) with an elliptical contact. While the point and elliptical contacts successfully generate adhesive wear failures (i.e., galling, scuffing, scoring), they do not represent the pressure or geometry found in the majority of real applications. Typically, the pressures found in the genuine contacts are an order of magnitude lower than those achieved using a point contact. The high pressures cause rapid deterioration of the original surface topography, resulting in the experiment running on the subsurface or significantly disturbed surface. This substantially affects the magnitude, progression, and often the mode of adhesive wear that occurs (Ref 90). Thus, although the pin-on-disk configuration is very simple, it is limited to a fixed load and a single wear track, making it very restricted in terms of galling evaluation. The modified cylinder-on-cylinder test (Fig. 14b) allows the possibility of scanning the contact load; however, it is still limited to a single wear track, thus making the analysis of the history of the contact surface impossible (Ref 89).

Another often unrecognized problem in lubricated wear testing aimed at analyzing scuffing wear failure is that when one surface is stationary and the other is moving, as is the case in most reciprocating sliding tests, any increase in sliding speed also leads to a corresponding increase in entrainment speed and thus EHD film thickness. This relationship only breaks down when heat generation due to sliding is so great that it reduces the effective viscosity of the lubricant in the contact inlet. This means that as the sliding speed is progressively increased in most scuffing tests, the thickness and strength of the EHD film also increases, complicating interpretation of the scuffing results obtained over a range of sliding speeds (Ref 91). It also means that lubricants of higher viscosity will tend to show higher resistance to scuffing than those of lower viscosity, regardless of the presence of boundary-lubricating additives. One way around this problem was suggested by Blok in a paper from 1946 (Ref 92); and alternative for rotating bodies given by Wedeven (Ref 93). Blok employed a rolling-sliding contact in which the two rubbing surfaces move in opposite directions relative to the contact. This enables the entrainment speed and the sliding speed to be decoupled, resulting in a very low entrainment speed and thus negligible fluid-film entrainment (Ref 91).

More application-oriented test methods include the twist compression test, originally developed in the 1970s to screen lubricants for sheet metal forming (Ref 94), and a strip-reduction (Ref 95) or strip-drawing test method, developed by Hirasaka and Nishimura (Ref 96), to directly simulate sheet metal forming processes and loads with geometrically simple tools. Another option for studying the galling resistance of tool steels for cold forming was presented by van der Heide et al. (Ref 97) and used a slider-on-sheet or a slider-on-flat-surface (Ref 58) test rig with a disk-shaped slider sliding against the sheet material in an infinite manner. A line-contact testing method aimed at simulating the contact between a piston ring and a cylinder liner was proposed by several authors (Ref 90, 98, 99), in which a roller bearing or an actual segment of the piston ring was placed in reciprocating sliding contact with a plate operating under starved lubrication or dry sliding. A novel approach to galling testing was developed by Hogmark et al. (Ref 89, 100) and used two crossed cylinders forced to slide against each other at a constant speed, with the normal force gradually increasing during sliding.

Twist Compression Test

The twist compression test (Fig. 15) uses the frictional force or coefficient of friction as the measured parameter that indicates adhesive failure or galling. As mentioned, the major use of the twist compression test is to screen lubricants to prevent adhesive transfer of the formed material to the tool surface. Type D2 tool steel in the form of an annular ring is often used for the "tool" tribological component, which is then rotated against the sheet material of concern (the type and thickness being studied), which was previously coated with the lubricant under study (Ref 55). The frictional force versus sliding distance is recorded, and the test is stopped when the frictional force recording shows a sudden increase or

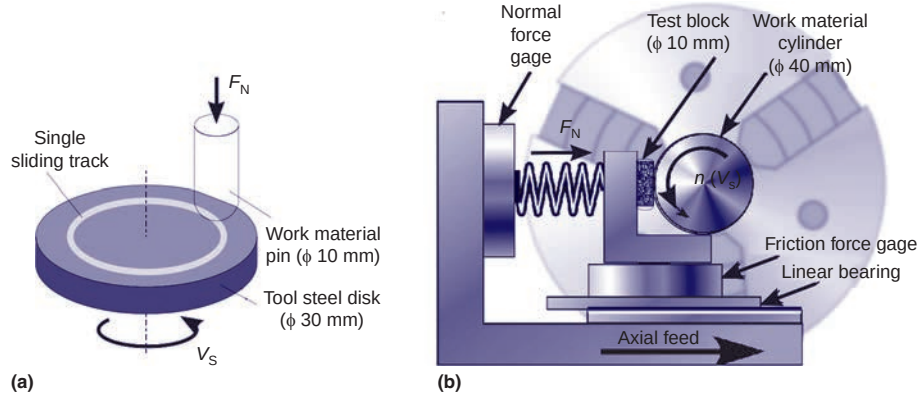

Fig. 14 Principal test setups for evaluating galling resistance. (a) Pin-on-disk test. (b) Modified cylinder-on-cylinder test. Adapted from Ref 89

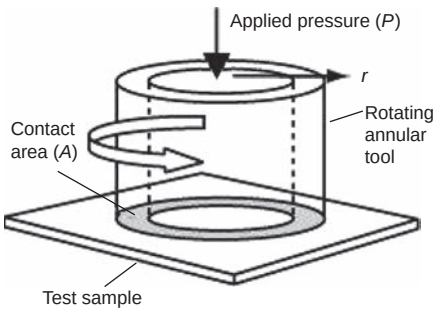

Fig. 15 Twist compression test setup. Source: Ref 101

perturbation, indicating adhesive failure in the form of excrescences, incipient galling, adhesive transfer, or other adhesive wear incidents. An adhesive wear event (i.e., scuffing) can be defined as a sharp increase in the coefficient of friction above 0.25 and lasting for two or more seconds (Ref 91). The sliding distance to failure and the apparent contact stress at the point of stopping are the test metrics. The lubricant that allows the highest sliding distance and apparent contact stress before adhesive failure (material transfer/galling) represents the best choice for a given material pair.

Slider-on-Flat-Surface Test

A test related to the contact situations in cold forming and sheet metal forming should first of all consist of a well-defined contact between the sheet material and the tool material, with the sliding distance being in the kilometer range. More importantly, the sheet material in contact should stay fresh, and the tool should be allowed to run in (Ref 97). These aspects are well combined in the slider-on-sheet or slider-on-flat-surface (Ref 58) configuration shown in Fig. 16; it allows an evaluation of the galling resistance of tool steels for cold forming. In this test, a disk-shaped tool material (10 mm, or 0.4 in., wide; 50 mm, or 2.0 in., diameter; 5 mm, or 0.2 in., edge radius) is forced to slide against the sheet material at a constant normal load, ranging up to 1000 N (225 lbf), and slid for up to 1000 mm (40 in.) at a fixed sliding speed (0.001 to 1 m/s, or 0.003 to 3.3 ft/s). During sliding, the tool is clamped to prevent it from rotating. At the end of each stroke, the tool is lifted, returned to the starting position, and moved a distance of 1 mm (0.04 in.) in the direction perpendicular to sliding. Subsequently, the normal force is reapplied and the next stroke made. By using the described routine, a fresh sheet surface is always in contact with the tool surface, similar to the conditions found in real forming operations (Ref 52). In this way, a 1 km (0.6 mile) sliding distance can be realized on 1 m^2 (11 ft^2) of sheet material (Ref 97).

Load-Scanning Test

Podgornik et al. (Ref 89) performed a study to evaluate the galling properties of tool materials for metal-forming operations, comparing several tribological laboratory test methods (pin-on-disk, block-on-cylinder, load scanner). Among several possibilities, it was proved that load scanning is a very simple and suitable method to evaluate the galling properties of tool materials. This method was successfully applied to study the effect of different coatings and surface-engineering techniques, surface treatments, and the roughness of the tool material (Ref 89), as well as the behavior of different lubricants (Ref 60, 61, 70, 102). The results can be analyzed in terms of the coefficient of friction, friction increase, material-transfer intensity, and critical loads for galling initiation and transfer-layer buildup (Ref 89). In addition to being very simple, load scanning also provides results representing a whole range of loads during a single test run. Furthermore, setting the equipment to multicycle mode offers a very rapid and convenient means of establishing friction maps, that is, diagrams of friction versus load and the number of strokes (Fig. 17).

The load-scanning test is conducted with two cylindrical specimens positioned in a cross-relative layout, that is, with the axes in perpendicular directions (Fig. 18). In this method, the upper vertically loaded cylinder (normally representing the tool material) is stationary, and the lower cylinder (representing the work material) is moved linearly (Ref 103, 104). The relative sliding motion during testing is 45° relative to each specimen axis; therefore, the contact spot, being of point-contact geometry, moves along a contact path on each specimen (Ref 60, 61, 70, 74, 89, 100). The test can be made with a constant normal load of up to a few kilonewtons, gradually increasing the load using a spring-based or pneumatic loading system (Ref 89, 103, 104) or varying the load using different loading waves during the test, facilitated by a precise numerical control (Ref 102). The sliding speed is another test parameter that can be adjusted; moreover, tests can be made by applying single or multipass conditions at room or elevated temperatures. Due to the specific cross-cylinder layout, each point along the contact path of both specimens will experience a unique load and display a unique tribological history after completion of the test (Ref 89).

Scratch Test

To study the galling process at the micro level, as well as its initiation, a displacement-controlled scratch test can be used. This involves a typical scratch tester with a diamond tip or a custom setup developed using a semiautomatic milling machine (Ref 105). The scratch test has several advantages, including the ability to investigate galling under a short sliding distance using the controlled depth of the penetration settings, continuous recording of the tangential force and acoustic emission (AE) data at a high sampling frequency, and surface examination of the workpiece samples with an optical profilometer to quantify the wear features in terms of the sliding distance. For the galling conditions, the tangential force was found to be unstable and of higher magnitude than for the nongalling conditions. Thus, the transition from nongalling to galling conditions can be actively monitored by studying the level and initiation of the unstable force and the presence of AE burst signals (Ref 105).

Sheet Metal Forming Simulation

Assessment of the coefficient of friction during sheet metal forming operations is a very complex task, with laboratory simulation tests representing a fundamental tool for obtaining the friction results. Tisza and Fülöp (Ref 106) classified tests for sheet metal forming as a function of these main operations:

- Stretch forming
- Deep drawing
- Stretch drawing

Stretch-forming and strip-reduction tests were used by several authors (Ref 95, 107–109) to study the influence of die material,

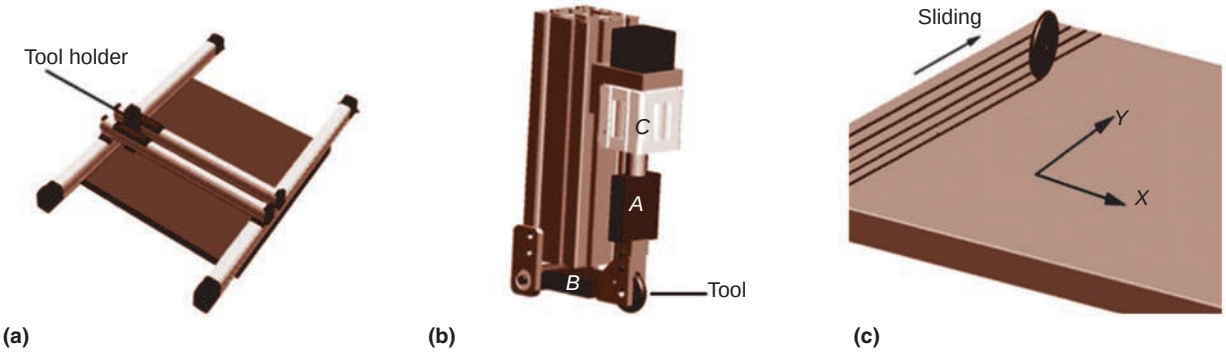

Fig. 16 Slider-on-flat-surface testing rig. (a) Overview. (b) Tool holder with load cells and actuator (A, normal load; B, friction force; C, load actuator). (c) Testing progression. Adapted from Ref 52

surface treatment, surface roughness, lubricant viscosity, as well as sheet material on friction during sheet metal forming. On the other hand, instrumented deep-drawing tests are mainly used to evaluate the effect of lubricants (Ref 82, 110, 111), while stretch-drawing-type tests are widely used to investigate the influence of different materials and technological parameters (Ref 112–115). Among the stretch-drawing tests, the draw-bead-type test introduced by Nine (Ref 116) plays a leading role.

Draw-Bead Test

The draw-bead test allows the simulation of bending and unbending in a sheet metal forming process and a measure of the coefficient of friction during sliding of the sheet material against a die in the forming process (Ref 117). Using proper test equipment, designed tests can be carried out in conjunction with a classic electromechanical or servohydraulic tensile test machine, thus allowing measurement of the forces associated with the forming process. The configuration is shown in Fig. 19, with the tests commonly performed at a constant speed (i.e., 1 mm/s, or 0.04 in./s), constant pulling and normal forces, and a total sliding distance of approximately 100 mm (4 in.) (Ref 74).

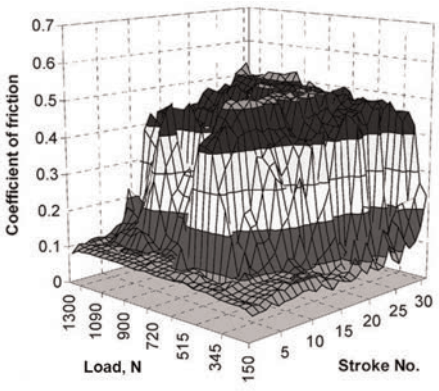

Fig. 17 Typical friction map obtained with a load-scanning test. Source: Ref 89

The pulling force of the sheet is the sum of the bending force and the frictional force. Thus, to determine the coefficient of friction in the forming process, it is important to define the contribution of each component to the pulling force. To resolve these, two types of tests are required. The first one, the A-type test, is made with the rolling elements being built with bearings. In this assembly, the pulling-force measurement takes into account only the deformation force, with the friction being negligible. In the second type of test, the B-type test, deformation rolls (numbered 1, 2, and 3 in Fig. 19a) are changed to fixed ones. In this case, the pulling-force measurement takes into account the deformation and the frictional force. The coefficient of friction is then calculated according to (Ref 116):

$$\mu = \frac{F_p - F_{pf}}{F_N} \qquad \text{(Eq 3)}$$

where F_p is the total pulling force; F_N is the normal force, acquired in the B-type test; and F_{pf} is the pulling force without friction, acquired in the A-type test.

In addition to the draw-bead test, a simulative tensile strip test (Ref 118) (which is widely used to measure the coefficient of friction) can provide further information about the behavior of the lubricant and sliding of the metal sheet over a punch. In this case, a metal sheet strip is placed over a cylindrical pin surface for drawing and stretching processes (Fig. 20). As the test strip is pulled on one side, the strain and force are measured on the other side. The coefficient of friction is then calculated using the Capstan model and the measured strip tension (Ref 119), and the pin surface is examined after the test.

Strip-Reduction Test

The strip-reduction test is a simulative test in which the process conditions of ironing can be replicated by reducing the thickness of a plane sheet strip. Ironing is considered to be one of the most severe of the sheet metal forming processes due to the occurrence of high localized pressures and large surface expansion. Unless very efficient boundary lubricants are applied, the combination of high localized pressures and stretching of the lubricant along the tool/workpiece contact interface gives rise to lubricant breakdown, material pickup, and galling (Ref 95). It is important to model both forward and backward strokes because in some industrial conditions the elastic expansion of the ironing die during the forward stroke helps to maintain the lubricant film on the contact surface, whereas the elastic contraction of the die before the backward unloading stroke results in severe contact conditions with possible lubricant-film breakdown and heavy material pickup. Figure 21 shows the design of the strip-reduction test tool with its main components, developed at the Technical University of Denmark (Ref 95). The forward stroke of the ironing process is replicated by drawing a strip (1) from right to left, while its thickness is reduced by means of two stationary cylindrical tool pins (2, 3). The upper cylindrical tool pin is located in a housing (4), which is placed on the base (5), and the base is mounted to the universal tribotester by means of guiding keys (6). The desired thickness reduction can be adjusted by changing the thickness of the shims (7). The lower cylindrical tool pin is mounted on a heater block (8), with which the tool temperature can be adjusted. The backward stroke of the ironing process is replicated by the second set of stationary cylindrical tool pins (9, 10), with a housing (11) and a heater block (12) providing the capability for tool-temperature adjustment. A torque transducer (13) is connected to the upper cylindrical tool pin, simulating the backward stroke.

The prevented access to the sheet/tool contact interface in sheet metal forming testing requires an indirect measurement in order to detect the onset of adhesive or galling wear failure. Conventional techniques (e.g., measurement of the frictional force) were found to have certain limitations, especially in terms of sensitivity when it comes to detecting the onset and first signs of material transfer. On the other hand, AE has been successfully

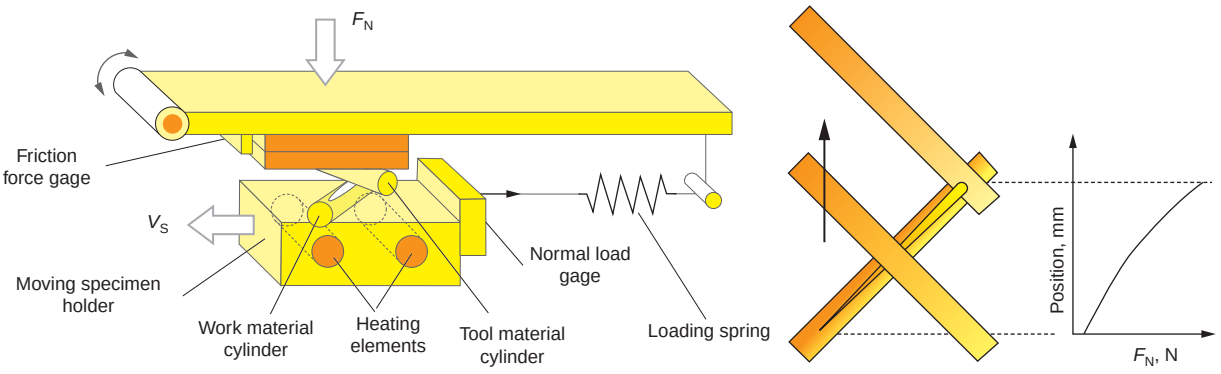

Fig. 18 Load-scanning test setup. Adapted from Ref 89

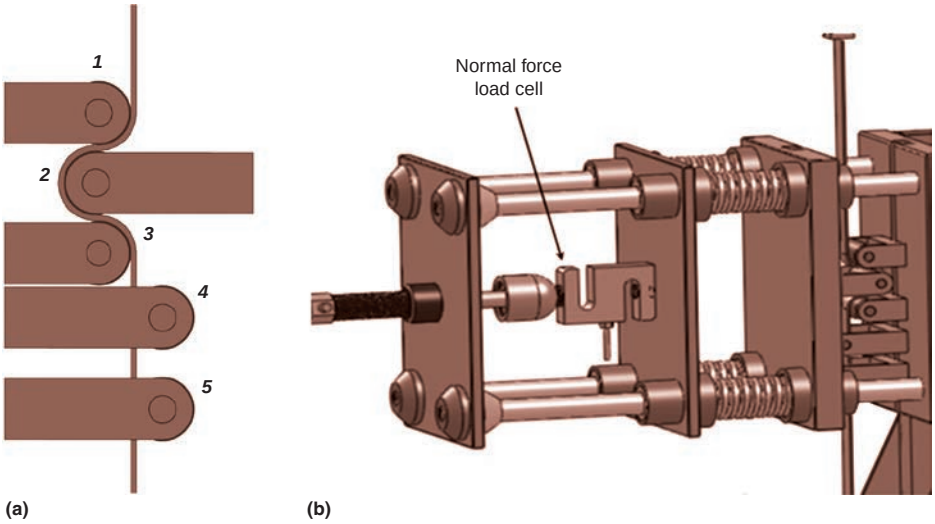

Fig. 19 Draw-bead friction test. (a) Configuration of deformation geometry. (b) outline of the test assembly. Adapted from Ref 74

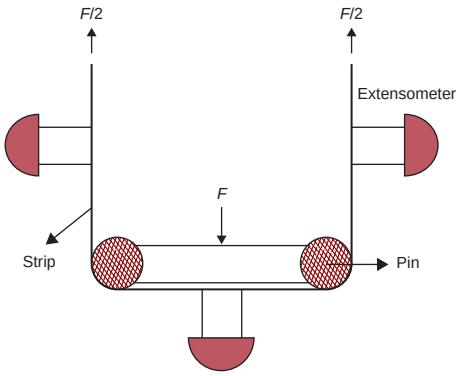

Fig. 20 Configuration of tensile strip test. Adapted from Ref 118

applied as an online monitoring technique for the evaluation of different tribological characteristics in metal-forming operations (Ref 120). Mostafavi et al. (Ref 121) successfully applied the AE technique to detect the onset of galling, noting a direct relationship between the wear mechanism and the AE peak amplitude. Furthermore, Moghadam et al. (Ref 122) showed that AE can be applied as an indirect, nondestructive measuring technique for the assessment of galling in strip-reduction testing. Testing that resulted in severely scored surfaces generated a large number of AE events, while the creation of a smooth surface had a significantly lower level of activity. A direct correlation between the contact conditions, lubricant performance, galling initiation, and generated AE events was identified, and the AE methodology was found to be suitable for online monitoring of galling in sheet metal forming (Ref 122).

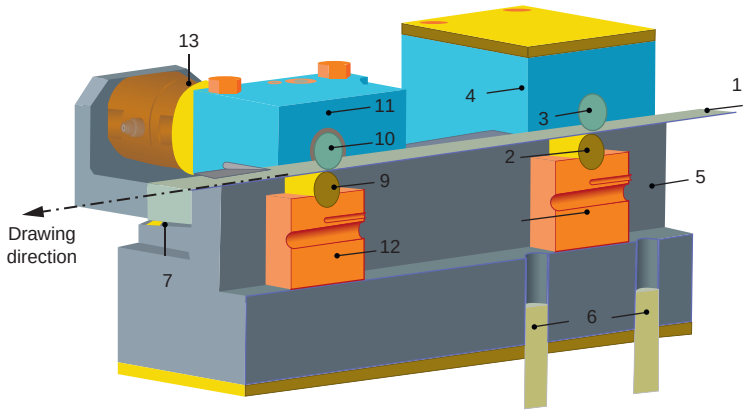

Fig. 21 Strip-reduction test tool design with its main components. See text for description. Adapted from Ref 95

Scuffing Testing

Laboratory-Scale Tests

Laboratory-scale scuffing tests are performed using several configurations as well as different procedures. Typical configurations that are well known and established in tribological testing include:

- Four-ball (Ref 123)
- Pin-on-twin (one cylinder reciprocating on two) (Ref 124)
- Ball-on-flat (reciprocating and rotating) (Ref 87)
- Cylinder-on-plate (pivoting) (Ref 125)
- Pin-on-disk/block-on-ring (rotating) (Ref 47, 126)
- Twin-disk type of setup (rolling/sliding) (Ref 127, 128)

These configurations have been widely used due to the relatively easy and accurate control of the contact parameters. Recently, a new approach to the laboratory scuffing test has been presented, using a ball-on-disk test device with contrarotating surfaces to limit EHD film formation (Ref 91). This arrangement makes it possible to determine the boundary-lubrication conditions over a wider range of sliding speeds. On the other hand, with the twin-disk test device (Fig. 22), the elliptical pressure distribution found between the gear teeth (e.g., in spiral bevel gears) can be successfully reproduced (Ref 129, 130). This is done through the precise definition of the geometries of the disks. The twin-disk test arrangement is well suited to studying scuffing under dynamic loading as well as running-in (Ref 41).

Most test procedures include an increase in the severity of the sliding contacts, for example, by an increase in the speed (Ref 132), load (Ref 47, 87), or by starved lubrication (Ref 126). However, there are also procedures that do not include any increase in severity and are simply based on performing the sliding test for a certain time or reaching a certain sliding distance (Ref 124, 125). In such cases, the experiments are normally started under lubricated low-load conditions using one drop of oil, which provides a proper running-in procedure before performing the actual scuffing test under starved lubrication.

The most commonly used scuffing test procedure is to increase the load stepwise while maintaining the surface velocities (rolling and sliding) constant until the scuffing failure occurs. The measurements during the test are usually limited to the frictional force and the bulk temperature of the contacting surfaces, because the localized maximum surface temperatures are not feasible to measure (Ref 35). Thus, in most tests, scuffing is considered to occur when the coefficient of friction increases and reaches a specific limit (Ref 133). Qu et al. (Ref 134) reported that the average coefficient of friction normally obtained in reciprocating sliding tests was not sufficiently sensitive and instead used the concept of analyzing local changes in the friction. On the other hand, Blau et al. (Ref 125) introduced a multiple scuffing criteria approach,

taking into account the frictional force, wear, and resulting surface roughness. Based on correlation with the visual assessment rankings, the R_a surface roughness parameter was found to give the most accurate measure of galling wear severity (Ref 65). Another option is to predict the critical scuffing temperature by using a thermal mixed elastohydrodynamic lubrication (EHL) model and a heat-balance model, which are used iteratively such that the heat generated at the contact interface predicted by the thermal mixed EHL model is an input for the heat-balance model, whose surface bulk temperature prediction is fed back into the thermal EHL analysis (Ref 35). In this way, the coefficient of friction, surface bulk temperature, and instantaneous local temperature can be predicted, allowing the identification of scuffing failure.

Gear Scuffing Tests

In the case of gears, scuffing-resistance testing (also known as the scuffing load-carrying-capacity test) (Ref 41) of the particular oil and/or material combination is performed by gear scuffing tests using an FZG machine (Fig. 23). In this case, two spur gear geometries can be used: type A gears, 10 and 20 mm (0.4 and 0.8 in.) wide (referenced as A10 and A20); and type C gears, 14 mm (0.55 in.) wide (referenced as C14) (Ref 136, 137). Several different types of tests can be performed, including:

- Standard load-carrying-capacity test (according to DIN 51354, A/8, 3/90)
- Variable-torque tests
- Variable-temperature tests
- Variable-speed tests, where the other two parameters are kept constant (Ref 138–140)

The results are then evaluated in terms of the load stage in which global and local scuffing occurs (Ref 138). The evolution of tooth-surface damage during a scuffing test is shown in Fig. 24. The global scuffing criterion defines gear scuffing as a failure that occurs on the macroscale (in a significant part of the meshing line), in which a critical average value of the power dissipation per unit area is exceeded. This critical value is proportional to the difference between the critical temperature of the lubricant and the temperature of the oil bath. On the other hand, the local scuffing criterion assumes that gear scuffing is initiated at the roughness asperity level (microcontact) when a lubricant-dependent critical value of the power dissipation per unit area is reached, without the need to define the critical temperature of the lubricant (Ref 138). The local scuffing criterion concept is used to explain scuffing initiation and the global concept for scuffing progression. When adequate running-in occurs and the operating conditions generate high contact pressures, the local and global concepts are compatible, predicting the occurrence of gear scuffing. The advantages and disadvantages of the local and global scuffing criteria are listed in Table 1 (Ref 138).

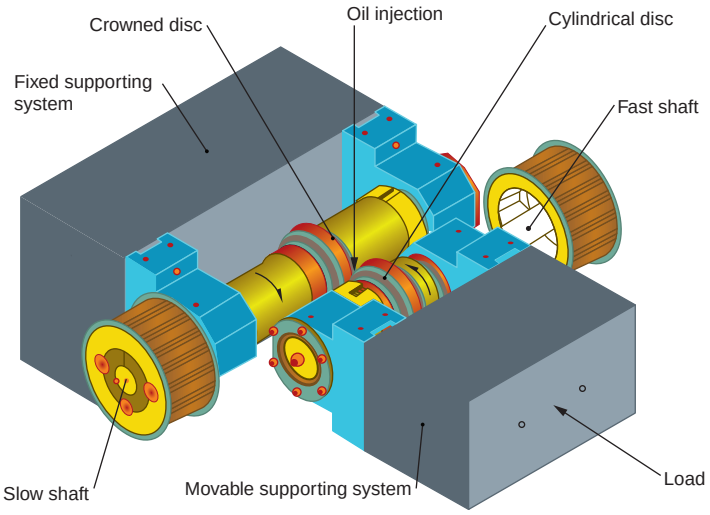

Fig. 22 Schematic of twin-disk test device. Adapted from Ref 131

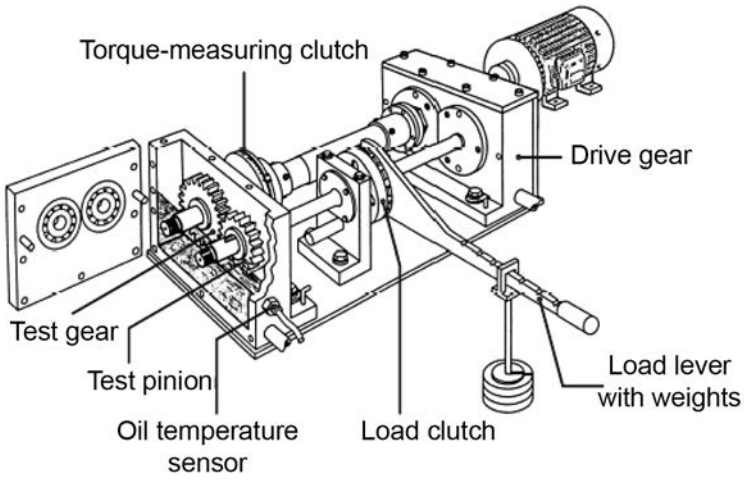

Fig. 23 Schematic of FZG back-to-back gear scuffing test setup. Source: Ref 135

With the development of new, advanced materials, and especially high-load-carrying-capacity oils, the resolution of the original FZG gear scuffing test (DIN 51354, A/8, 3/90) became insufficient for adequate testing and screening. To overcome this limitation, FZG developed a new method called the scuffing shock test, denoted as S-A10/16, 6R/90 or S-A10/16, 6R/110 (S = shock), depending on the initial oil temperature (90 or 110 °C, or 195 or 230 °F) (Ref 141). The scuffing shock test is carried out under much more severe contact conditions compared to the A/8, 3/90 standard test. This is a result of the reduced face width of the pinion, the double rotational speed, the higher initial oil temperature, the reverse direction of rotation, and the start of the test at the load for which the scuffing failure is expected, thus the name "shock test." Shock loading prevents the test gears from running-in and, in turn, increases their susceptibility to scuffing, thus increasing the resolution of the method (Ref 142). A further increase in the oil temperature to 120 °C (250 °F), as proposed by Tuszynski et al. (Ref 142), is expected to provide a suitable method for testing the scuffing resistance of low-friction, carbon-base, wear-resistant coatings.

In addition to the FZG scuffing test procedure, several gear scuffing studies have been performed with bevel-gear-based test devices (Ref 143, 144). However, despite the stability of the results delivered by gear-based test stands, the possibilities for investigating a wider range of contact and/or material parameters are somewhat limited, often requiring a new design for the gear wheels (Ref 41). In such cases, more basic research using laboratory-scale scuffing test procedures and test rigs is preferred.

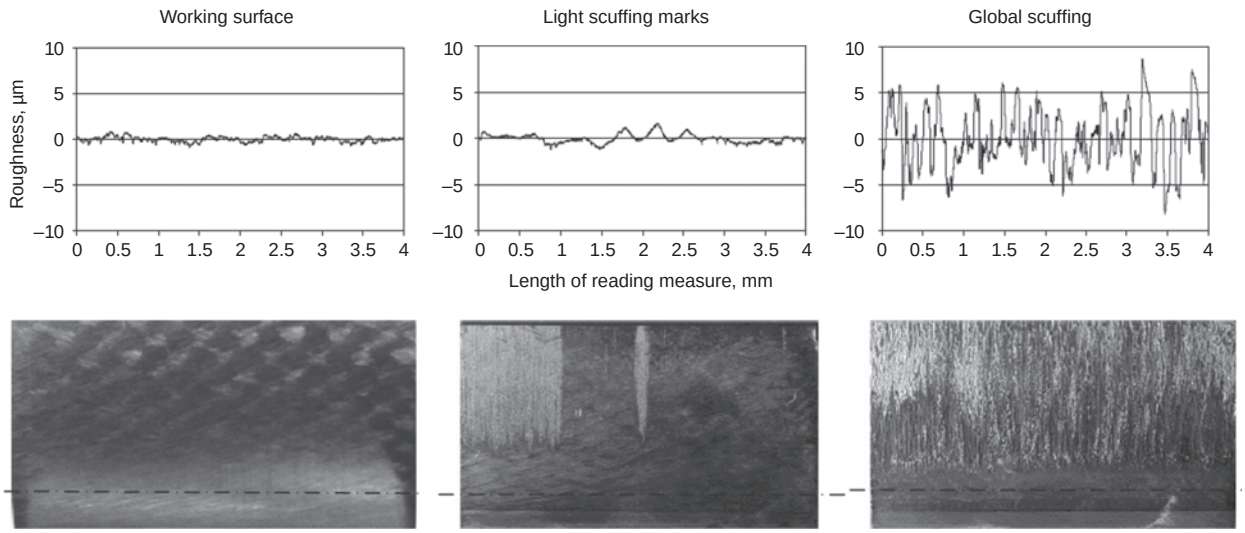

Fig. 24 Evolution of tooth-surface damage during a scuffing test. Reprinted from Ref 138 with permission from Elsevier

Piston Ring and Cylinder Liner Contact Simulation

The common approach to testing piston ring and cylinder liner materials is to run a fired-engine test bench. However, in addition to being expensive, it does not allow a detailed investigation of the effect of different contact parameters. The major advantage of using the test procedure of the model with a reciprocating sliding line contact is the opportunity to adjust each contact parameter independently. For the model test simulating scuffing in the piston ring/cylinder liner contact, an SRV machine (Optimol Instruments Prüftechnik GmbH), TE-77 (Phoenix Tribology Ltd.), or similar device providing a line reciprocating sliding contact can be employed, allowing precise control of the normal force, temperature, and stroke as well as the lubrication mode. With the reciprocating setup of the test device, the movement pattern of the piston ring at the fired top dead-center position is represented in a controlled environment (Ref 145).

The SRV test rig and setup also allows the use of different tilt angles to better control the lubrication situation. In this case, a cylinder liner segment is mounted inside the test chamber on a fixed, heatable sample holder equipped with a friction-force sensor. A piston ring segment is inserted into a movable ring sample holder driven by an electric drive that reciprocates parallel to the liner surface and is loaded with a top-loading unit. The setup allows control over the liner temperature, stroke and frequency of the piston ring segment, normal load, and oil supply rate. Normally, the test procedure is divided into two main parts: the starting procedure and the test itself (Ref 145). The starting procedure consists of heating the samples and obtaining the equilibrium temperature field, followed by starting the oil flow supply with preloading, which ensures the same starting conditions for each individual test. After the starting procedure, the main test (including the reciprocating movement) is started, employing a fixed-load or increased load-carrying-capacity procedure. The tests are then evaluated in terms of the stability of the coefficient of friction. If the coefficient of friction exceeds 0.3 for more than 30 s, the test is defined as failed, experiencing scuffing failure; otherwise, the test can be defined as passed as a stable pass test for cases with a very stable coefficient of friction signal, and as an unstable pass test for cases with a lot of noise and instability in the coefficient of friction signal (Ref 145).

Table 1 Advantages and disadvantages of local and global scuffing criteria

Advantages	Disadvantages
Local scuffing criteria	
Predicts gear scuffing during running-in	Complex numerical model
Efficient at low and high oil temperatures	Large number of calculations
Explains the appearance of the first scuffingmarks in localized zones along the meshingline	Very sensitive to load-share function (not applicable for high-load, low-speed conditions)
Global scuffing criteria	
Simple application	Definition of average coefficient of friction required
Very efficient for stable operating conditions (after running-in, high contact pressure, low oil temperature)	Does not predict gear scuffing during running-in
	Inefficient at high oil temperatures
	Does not explain the appearance of the first scuffing marks

Source: Ref 138

Material-Dependent Adhesive Wear

Investigations of sheet metal forming (Ref 146) have shown that the critical contact pressure at which severe adhesive wear in the form of galling occurs correlates with the proof stress of the sheet material and the microstructure of the tool. Galling normally occurs at higher contact pressures for the high-strength sheet material (i.e., metastable austenitic sheet material), while sliding against a low-strength material (i.e., EN 1.4301) results in galling at lower contact pressures (Ref 146). Furthermore, compared to the classic ingot-cast, electroslag-remelted, and forged tool steels, the powder metallurgy (PM) tool steels with homogeneously distributed carbides and carbonitrides and higher hardness show much better galling resistance, resisting galling at higher contact pressures against different steel sheet materials (Ref 64, 146). At critical pressures, the plasticized sheet material slides along the tool (causing accelerated wear of the tool matrix), which, in turn, promotes extensive sheet-material transfer and lump formation. In this case, homogeneously distributed fine carbides and carbonitrides prevent the penetration of the sheet material into the tool matrix, with lower plasticity of the sheet material further reducing the contact area and the likelihood of galling initiation. On the other hand, for randomly, nonhomogeneously

distributed elongated carbides in conventional tool steels and high plasticity of the sheet material, the sheet material can be pressed down, reaching relatively large areas of the tool-steel matrix and thus promoting galling (Ref 146).

Besides the homogeneity of the hard-phase distribution, adhesive and galling wear resistance in forming was found to be strongly dependent on the chemistry of the tool steel and phase composition (Ref 52). As shown in Fig. 25, the amount of carbides is an important parameter for tool life and resistance to galling. The tool steel material without any primary carbides does not withstand any sliding without wear and is completely worn out by the combination of abrasive and adhesive wear. Increasing the primary carbide amount to 12 vol% leads to some improvement in the sliding distance to galling against sheet steel material, although it is still relatively short. A further increase in the primary carbide content to approximately 20 vol% leads to a significant increase in galling resistance (Ref 52, 147). Interestingly, very similar results in terms of galling resistance are observed for different types of carbides (M3 and M4 in Fig. 25) as long as the volume fraction of carbides remains constant. However, compared to the carbides, the carbonitrides were found to provide further improvement in galling resistance, with the PM tool steels containing only carbonitrides being superior, showing hardly any signs of galling (Ref 52, 148–151). Superior adhesive and antigalling wear resistance for carbonitrides was confirmed by investigation of nitrided tool steels, showing a further reduction in galling (Ref 66). Thus, both chemical composition and amount of reinforcement particles, including the size and interparticle distance (the smaller the better) (Ref 58), are important parameters in terms of adhesive and galling wear resistance (Ref 52), with the reinforcement particles showing a much lower adhesion tendency than the metallic matrix (Ref 152). However, change in the work material can lead to completely different results when forming soft materials such as Al and Al alloys; the surface roughness and irregularities become dominant, promoting initial material transfer. Obviously, a high density of protrusions/valleys at a slightly different level (on a nanometer scale) than the surrounding metal matrix, as associated with fine hard-phase particles in PM tool steels, will increase tribological interaction with the softer counter-surface, damage the native oxide surface films, and intensify the tendency for initial material transfer (Ref 57). The interlocking action, more pronounced for harder and more protruding hard-phase particles, that is, M(C,N), also leads to increased friction (Ref 67).

In terms of chemical composition, vanadium (which is an important lubricious surface oxide formed, especially when in the form of vanadium nitrides) provides outstanding friction and wear properties for tool steels (Ref 153). The very high galling resistance of nitrogen-alloyed, vanadium-containing PM tool steels found under the dynamic conditions in tool/work material interactions is due to the strong presence of lubricous Magnéli-type oxides (V_2O_5) that form on the VN, VC, and V(C, N) precipitates.

In sheet metal forming, adhesive wear rate and tool wear resistance also depend strongly on the sheet material, not only on its strength but also on the metallurgical composition (Ref 154). The results of Schumacher (Ref 155, 156) show the relatively low galling resistance of austenitic and precipitation-hardened stainless steels, while the remaining standard stainless steel alloys exhibit far better galling resistance in different combinations. These results demonstrate the detrimental effect of high nickel content on galling resistance, unless the alloy is further modified specifically for galling resistance (Ref 155). Further improvements in adhesive wear resistance can be achieved by altering the surface characteristics by nitriding or alloying with aluminum instead of sulfur. Thus, AISI 303MA-type stainless steel shows a surprisingly high level of galling resistance compared to type 303.

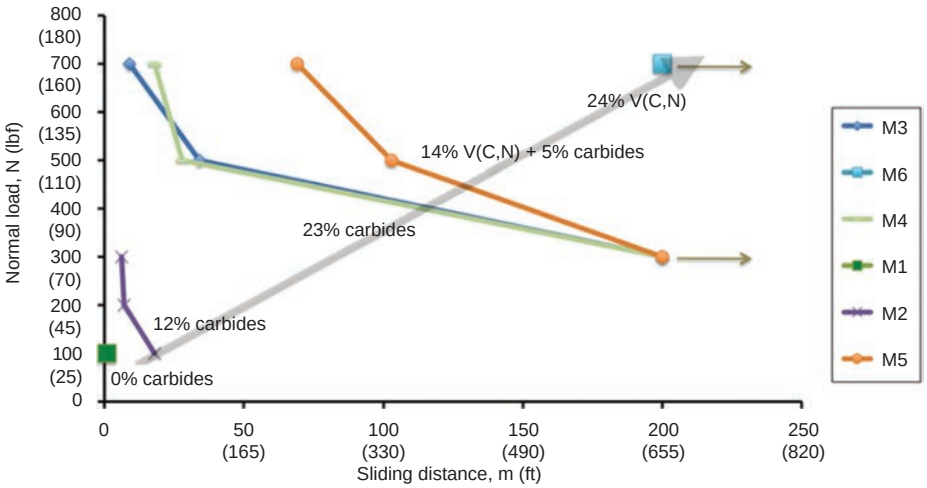

Fig. 25 Critical sliding distance to galling for different reinforcement particle types and content. Source: Ref 52

Summary

The number one material property that promotes adhesive wear is probably plasticity, the ability of a material to plastically deform under sufficient stress (Ref 55). For a material to flow up and form a protrusion from surrounding material, it must have the ability to plastically deform; therefore, it must have high ductility. A quantitative measure of the ability of a material to plastically deform is its plasticity index, which is the slope of the plastic region of a true stress/true strain curve (Ref 157). As such, plasticity indexes or strain-hardening coefficients can correlate with the tendency of a material to exhibit adhesive wear. This concept suggests that brittle ceramics do not plastically deform like metals, and thus, they should be less prone to adhesive wear failures. Furthermore, the work of Schumacher (Ref 55, 156–159) suggests that metals with a low stacking-fault energy are more prone to severe adhesive wear failures (i.e., galling) than those with a high stacking-fault energy. Adhesive transfer in metals was also found to be related to the ability of metals to solid-state weld under the action of rubbing, with self-mated metals being more prone to friction weld to each other than metals that do not form solid solutions (Ref 9). Some metals are known to form strong junctions, and this tendency is related to the metallurgical solid solubility.

In the case of tool steels, the major factor influencing adhesive wear resistance is the hard phase (i.e., precipitates such as carbides, carbonitrides, and nitrides); this includes the type of hard particles, the size, and the distribution. Improved adhesive and galling wear resistance is obtained by using high volume fractions of small, homogeneously distributed hard particles with a small interparticle distance, preferably of the nitride or carbonitride type (Ref 52). Generally, the improvement is attributed to a fine homogeneous dispersion of small precipitates possessing low adhesion against different sheet materials and reducing the contact with the metallic matrix (Ref 64, 160). However, a large hardness difference between the hard-phase particles and the matrix can result in larger protrusions of these hard phases above the matrix when polished and thus in increased interlocking with the sheet material, increased friction, and consequently a higher likelihood of increased adhesive wear (Ref 67).

In relation to the composition of the material, the formation of lubricious oxides (i.e., V_2O_5) or oxidized wear debris will result in the development of glaze layers that reduce the occurrence of adhesive wear failures

(Ref 66). The oxides and oxide films found on most metallic surfaces are good protection against adhesive wear. If lubrication fails or if the surfaces have to run in air without any lubricant, an oxide can prevent metal-to-metal contact on a significant scale (Ref 1). Also, contaminants and material impurities have a similar effect, reducing or even eliminating adhesion between solids (Ref 2). The oxidation of metals occurs rapidly, even at low temperatures, and the rate at which oxidation proceeds is often limited only by the supply of oxygen until the critical 5 nm thickness is reached (Ref 161). This means that under atmospheric pressure, oxide films, if removed, are reformed in just a few microseconds. This rapid regrowth means that a protective oxide film in a wearing contact can be sustained indefinitely, thus effectively preventing or minimizing adhesive wear.

In terms of changing the surface chemistry, Arai and Tsuchiya (Ref 162) found that diffusion treatments, especially nitriding, greatly improve adhesive wear resistance in forming and drawing operations. This indicates that the tribological properties and the adhesive wear resistance of contact surfaces can be further improved through the application of proper surface-engineering techniques (Ref 51, 61, 163). A tailored surface-engineering process, on one hand, increases the surface hardness of a contacting surface, while, on the other hand, it alters the chemical nature and thus effectively reduces the possibility of adhesion between the contacting surfaces (Ref 17). In recent years, the main focus on improving the galling resistance of forming tools has been on the use of hard coatings (Ref 61, 163, 164). While ceramic coatings used in cutting applications normally show a relatively high friction and strong tendency for galling, low-friction coatings (i.e., diamondlike carbon coatings, chrome plating, etc.) can give very stable friction and excellent galling resistance (Ref 60, 61, 155). In the case of diamond- and graphite-like carbon coatings sliding against steel, superior adhesive wear resistance can be attributed to the in situ formation of a transferred, low-shear, thin graphitic film, which blocks the creation of adhesive bonds between the contact surfaces (Ref 165, 166). However, coating selection is greatly influenced by the type of work material, with different surface treatments including nitriding and a deep cryogenic treatment providing similar or even better results when forming nonferrous alloys (Ref 167, 168). In any case, to restrain galling initiation, polishing of the tool surface is required in many forming operations. Even on coated surfaces, the initial transfer of work material to the tool surface is significantly reduced by substrate pretreatment and coating posttreatment (polishing), both resulting in a smoother contact surface (Ref 169). It is well known that the risk of adhesive wear failures, including galling, increases with surface roughness (Ref 170, 171). There are clear indications that the roughness and topography of the harder surface, even at the nano level, are the major factors in causing transfer from a softer countersurface (Ref 172). However, the more difficult the material is to form, the less pronounced is the positive effect of surface polishing (Ref 167). On the other hand, selection of the proper plateaulike topography and topography optimization can have a positive effect on the surface tribological performance (Ref 173). In particular, surface texturing, involving microdimples on the bearing surface, shows great potential in lubricated sliding contacts (Ref 70, 174, 175). When lubricated, dimples act as oil reservoirs and prevent adhesion through the formation of a thicker protective lubrication film, while for dry sliding, the adhesion is accelerated. However, when coated, the effect of surface roughness and topography also depends on the coating type. In the case of hard ceramic coatings, a smoother substrate and especially postpolishing of the coated surface can give up to two times better galling resistance, while for softer, low-friction coatings, substrate roughness and postpolishing have only a very minor effect (Ref 51).

Another important aspect of reducing adhesive wear in sliding contacts is the careful choice of sliding materials (Ref 2). The general rule is to avoid sliding similar or identical materials against each other (Ref 176). Strong arguments have been made that mutually soluble metals should not be slid against each other (Ref 177). Also, chemically active metals will show much stronger adhesion to iron than passive or inert ones. Examples of such metals with low chemical activity are lead, tin, copper, and noble metals, which are widely used as bearing materials in demanding applications to reduce friction and adhesive wear (Ref 13). On the other hand, impure, microstructurally heterogeneous materials are also less reactive than pure metals and therefore show better adhesive wear resistance (Ref 36). In the case of contacts with nonmetallic materials, such as polymers and ceramics, the friction behavior mainly depends on the nonmetallic counterpart, with polymers normally showing low friction and a low adhesion tendency. In contrast, ceramics sliding against themselves or against metals exhibit relatively high friction and high adhesive wear rates (Ref 178). Also, in tooling applications, the galling performance of the tool strongly depends on the work material (Ref 167). In the case of stainless steels, carbon-base coatings give superior galling performance. For aluminum, nitride-type surfaces show lower and more stable friction as well as the best protection against aluminum transfer. The most critical material in terms of galling seems to be titanium, showing high friction and almost immediate transfer to the tool surface. Some improvements are observed with plasma nitriding and vanadium nitride coating (Ref 167). As shown by Lugscheider et al. (Ref 179), a possible way of selecting the surface-engineering technique best suited to a certain work material could be through a measurement of the surface energy. Adhesion as a feature of the bonding between solids relies on semivalent forces, which can be divided into dispersed and polar components. When two solids make contact with each other, the only interaction at the interface is between the two polar and the two dispersed components of their interfacial tension. Therefore, the surface energy of a forming tool surface should be as low as possible, with its polar/dispersion ratio depending on the surface energy of the formed material (Ref 179).

Adhesive wear is best eliminated by preventing the metal-to-metal contact of sliding surfaces, which is most effectively established by lubricating the contact and using a lubricant with the appropriate viscosity. The primary purpose of a lubricant is to suppress adhesive wear by providing a superior form of surface contamination (Ref 2). Fatty acids and other polar organic substances are usually blended into lubricating oils. If these fatty acids adsorb on the top of the existing oxide layers, further reductions in friction and wear are obtained (Ref 176). Furthermore, machine components and forming oils also contain additives rich in sulfur, phosphorus, or chlorine, which can form sulfide, phosphide, or chloride protective films on metallic surfaces (Ref 13). These films are intended to form when the oxide films break down, to provide protective surface films against very high friction and adhesion. On the other hand, the presence of the lubricant can lead to hydrodynamic pressure buildup in the contact inlet, which can keep the contact surfaces completely separated, preventing any metal-to-metal contact (Ref 1).

The factors preventing adhesive wear can be summarized and categorized into groups (Ref 3, 6, 62, 70, 73):

- Controlling contact severity by avoiding shocks and elevated levels and by keeping load, speed, and temperature as low as possible
- Increasing the contact area to reduce the contact stress
- Using harder materials with a higher yield strength and alloys with a high adhesion resistance
- Using dissimilar contact materials
- Avoiding extremely smooth ($R_a < 0.05$ μm) or very rough ($R_a > 0.70$ μm) surfaces, which can promote adhesion; polishing contact surfaces, even after coating, is the most effective
- Having oxides on contact surfaces
- Implementing surface-engineering techniques
- Using solid lubricants
- Lubricating the contact and using higher-viscosity oils
- Using antiwear and extreme-pressure additives in the oil

REFERENCES

1. C.R. Gagg and P.R. Lewis, Wear as a Product Failure Mechanism—Overview and Case Studies, *Eng. Fail. Anal.*, Vol 14, 2007, p 1618–1640
2. G.W. Stachowiak and A.W. Batchelor, *Engineering Tribology*, 4th ed., Butterworth-Heinemann, London, 2013
3. D. Kopeliovich, "Mechacnisms of Wear," SubsTech—Knowledge Source on Materials Engineering, https://www.substech.com/dokuwiki/doku.php?id=mechanisms_of_wear# adhesive_wear, accessed Jan 10, 2019
4. R. Scott, Basic Wear Modes in Lubricated Systems, *Mach. Lubr.*, Vol 7, 2008, https://www.machinerylubrication.com/Read/1375/wear-modes-lubricated, accessed Jan 10, 2019
5. A. Devaraju, A Critical Review on Different Types of Wear of Materials, *Int. J. Mech. Eng. Technol. (IJMET)*, Vol 6 (No. 11), 2015, p 77–83
6. S.D. Nyman, "What Is Wear," C.C. Jenson, March 2007, https://www.cjc.dk/fileadmin/root/File_Admin_Filter/doc_Articles/What_is_Wear__2007.pdf, accessed Jan 10, 2019
7. C. Zhang, Understanding the Wear and Tribological Properties of Ceramic Matrix Composites, *Advances in Ceramic Matrix Composites*, I.M. Low, Ed., Woodhead Publishing, 2014
8. "Understanding Wear and Recognizing Different Wear Modes," AZO Materials, 2013, https://www.azom.com/article.aspx?ArticleID=9405, accessed Jan 10, 2019
9. E. Rabinowicz, *Friction and Wear of Materials*, 2nd ed., Wiley, New York, 1995
10. H. Krupp, Recent Results in Particle Adhesion: UHV Measurements, Light Modulated Adhesion and the Effect of Adsorbates, *J. Adhes.*, Vol 4, 1972, p 83–86
11. O. Vingsbo, Wear and Wear Mechanisms, *Proc. Int. Conf. on Wear of Materials*, K.C. Ludema, W.A. Glaeser, and S.K. Rhee, Ed., April 1979 (Dearborn, MI), American Society of Mechanical Engineers, New York, 1979, p 620–635
12. J.M. Ziman, *Electrons in Metals—A Short Guide to the Fermi Surface*, Taylor and Francis, London, 1963
13. D.H. Buckley, *Surface Effects in Adhesion, Friction, Wear and Lubrication*, Elsevier, 1981
14. M.E. Sikorski, Correlation of the Coefficient of Adhesion with Various Physical and Mechanical Properties of Metals, *Trans. ASME, J. Basic Eng.*, Vol 85, 1963, p 279–285
15. H. Hirani, "*Tribology—Adhesive Wear*," http://web.iitd.ac.in/~hirani/lec07.pdf, accessed Jan 10, 2019
16. K. Kato and K. Adachi, Wear Mechanisms, *Modern Tribology Handbook*, B. Bhushan, Ed., CRC Press, London, 2001, p 273–299
17. C.X. Li, "*Wear and Wear Mechanism*," http://emrtk.uni-miskolc.hu/projektek/adveng/home/kurzus/korsz_anyagtech/1_konzultacio_elemei/wear_and_wear_mechanism.htm, accessed Jan 10, 2019
18. T. Kayaba and K. Kato, The Adhesive Transfer of the Slip-Tongue and the Wedge, *ASLE Trans.*, Vol 24 (No. 2), 1981, p 164–174
19. T. Sasada, S. Norose, and H. Mishina, The Behaviour of Adhered Fragments Interposed between Sliding Surfaces and the Formation Process of Wear Particles, *Proc. Int. Conf. on Wear of Materials*, K.C. Ludema, W.A. Glaeser, and S.K. Rhee, Ed., April 1979 (Dearborn, MI), American Society of Mechanical Engineers, New York, 1979, p 72–80
20. O. Vingsbo and S. Hogmark, Wear of Steels, *Fundamentals of Friction and Wear of Materials*, D.A. Rigney, Ed., American Society for Metals, 1980, p 373–380
21. L.H. Chen and D.A. Rigney, Transfer during Unlubricated Sliding Wear of Selected Metal Systems, *Wear*, Vol 105, 1985, p 47–61
22. J.F. Archard, Single Contacts and Multiple Encounters, *J. Appl. Phys.*, Vol 32, 1961, p 1420–1425
23. R. Aghababaei, D.H. Warner, and J.-F. Molinari, On the Debris-Level Origins of Adhesive Wear, *Proc. Natl. Acad. Sci. USA*, Vol 114 (No. 30), 2017, p 7935–7940
24. R. Aghababaei, D.H. Warner, and J.-F. Molinari, Critical Length Scale Controls Adhesive Wear Mechanisms, *Nat. Commun.*, Vol 7, 2016, p 11816
25. R. Aghababaei, On the Origins of Third-Body Particle Formation during Adhesive Wear, *Wear*, Vol 426–427, 2019, p 1076–1081
26. D.-H. Cho, J.-S. Kim, J. Jia, and Y.-Z. Lee, Comparative Analysis Based on Adiabatic Shear Instability for Scuffing Failure between Unidirectional and Reciprocating Sliding Motion, *Wear*, Vol 297, 2013, p 774–780
27. "Factors Affecting Wear and Galling," British Stainless Steel Association, https://www.bssa.org.uk/topics.php?article=11, accessed Jan 10, 2019
28. J. Castro and J. Seabra, Influence of Mass Temperature on Gear Scuffing, *Tribol. Int.*, Vol 119, 2018, p 27–37
29. A. Dyson and L.D. Wedeven, "*Assessment of Lubricated Contacts—Mechanisms of Scuffing and Scoring*," NASA Technical Memorandum 83074, NASA, 1983
30. K. Gopinath and M.M. Mayuram, "Gear Failure," https://www.coursehero.com/file/15215391/2-8/, accessed Jan 10, 2019
31. "Gears and Scuffing Wear Review," Engineers Edge, https://www.engineersedge.com/gears/gear_scuffing_wear.htm,
32. L. Wojciechowski, M. Wieczorowski, and T.G. Mathia, Transition from the Boundary Lubrication to Scuffing—The Role of Metallic Surfaces Morphology, *Wear*, Vol 392–393, 2017, p 39–49
33. F. Saeidi, A.A. Taylor, B. Meylan, P. Hoffmann, and K. Wasmer, Origin of Scuffing in Grey Cast Iron-Steel Tribo-System, *Mater. Des.*, Vol 116, 2017, p 622–630
34. A. Dyson, Scuffing—A Review, *Tribol. Int.*, Vol 8, 1975, p 77–87
35. S. Li, A. Kahraman, N. Anderson, and L. D. Wedeven, A Model to Predict Scuffing Failures of a Ball-on-Disk Contact, *Tribol. Int.*, Vol 60, 2013, p 233–245
36. O.O. Ajayi, C. Lorenzo-Martin, R.A. Erck, and G.R. Fenske, Scuffing Mechanism of Near-Surface Material during Lubricated Severe Sliding Contact, *Wear*, Vol 271, 2011, p 1750– 1753
37. P. Olander and S. Jacobson, Scuffing Resistance Testing of Piston Ring Materials for Marine Two-Stroke Diesel Engines and Mapping of the Operating Mechanisms, *Wear*, Vol 330–331, 2015, p 42–48
38. P.J. Blau, "*Scuffing: From Basic Understanding to Engine Materials Testing*," DEER Conference, Aug 2007 (Detroit, MI), https://www.energy.gov/sites/prod/files/2014/03/f9/deer07_blau.pdf,
39. J. Hershberger, O.O. Ajayi, J. Zhang, H. Yoon, and G.R. Fenske, Evidence of Scuffing Initiation by Adiabatic Shear Instability, *Wear*, Vol 258, 2005, p 1471–1478
40. P. Groche and Y. Wu, Inline Observation of Tool Wear in Deep Drawing with Thermoelectric and Optical Measurements, *CIRP Ann. Manuf. Technol.*, Vol 68, 2019, p 567–570
41. M. Savolainen and A. Lehtovaara, An Experimental Approach for Investigating Scuffing Initiation due to Overload Cycles with a Twin-Disc Test Device, *Tribol. Int.*, Vol 109, 2017, p 311–318
42. S. Bair and W.O. Winer, Lubricant Shear Response to Large Strain at High Pressure, *J. Rheol.*, Vol 6, 1980, p 936–937
43. K.-B. Park and K.C. Ludema, Evaluation of the Plasticity Index as a Scuffing Criterion, *Wear*, Vol 175, 1994, p 123–131
44. J. Enthoven and H.A. Spikes, Infrared and Visual Study of the Mechanisms of Scuffing, *Tribol. Trans.*, Vol 39, 1996, p 441–447
45. W.F. Bowman and G.W. Stachowiak, A Review of Scuffing Models, *Tribol. Lett.*, Vol 2, 1996, p 113–131
46. K.C. Ludema, A Review of Scuffing and Running-In of Lubricated Surfaces, with

Asperities and Oxides in Perspective, *Wear*, Vol 100, 1984, p 315–331
47. O.O. Ajayi, J. Hershberger, J. Zhang, H. Yoon, and G.R. Fenske, Microstructural Evolution during Scuffing of Hardened 4340 Steel—Implication for Scuffing Mechanism, *Tribol. Int*., Vol 38, 2005, p 277–282
48. "Seizing," *NTN Global*, https://www.ntnglobal.com/en/products/care/damage/branded.html, accessed Jan 10, 2019
49. "How to Read a Damaged Piston," Madsen's Shop & Supply Inc., http://www.tmadsens1.com/saw_piston_fail.htm, accessed Jan 10, 2019
50. E. Heidevan der and D.J. Schipper, Galling Initiation due to Frictional Heating, *Wear*, Vol 254, 2003, p 1127–1133
51. B. Podgornik and J. Jerina, Surface Topography Effect on Galling Resistance of Coated and Uncoated Tool Steel, *Surf. Coat. Technol*., Vol 206, 2012, p 2792–2800
52. A. Gåård, Influence of Tool Microstructure on Galling Resistance, *Tribol. Int*., Vol 57, 2013, p 251–256
53. W.R.D. Wilson, Tribology in Cold Metal Forming, *J. Manuf. Sci. Eng*., Vol 119, 1997, p 695–698
54. L. Kirkhorn, V. Bushlya, M. Andersson, and J.-E. Ståhl, The Influence of Tool Steel Microstructure on Friction in Sheet Metal Forming, *Wear*, Vol 302, 2013, p 1268–1278
55. K.G. Budinski and S.T. Budinski, Interpretation of Galling Tests, *Wear*, Vol 332–333, 2015, p 1185–1192
56. A. Gåård, P. Krakhmalev, and J. Bergström, Influence of Tool Steel Microstructure on Origin of Galling Initiation and Wear Mechanisms under Dry Sliding against a Carbon Steel Sheet, *Wear*, Vol 267, 2009, p 387–393
57. J. Heinrichs, M. Olsson, and S. Jacobson, Influence of Tool Steel Microstructure on Initial Material Transfer in Metal Forming—In Situ Studies in the SEM, *Wear*, Vol 302, 2013, p 1249–1256
58. A. Gåård, P. Krakhmalev, and J. Bergström, Wear Mechanisms in Deep Drawing of Carbon Steel—Correlation to Laboratory Testing, *Tribotest*, Vol 14, 2008, p 1–9
59. S. Hogmark, S. Jacobson, and E. Coronel, On Adhesion in Tribological Contacts—Causes and Consequences, *Tribologia*, Vol 26, 2007, p 3–16
60. B. Podgornik, S. Hogmark, O. Sandberg, and V. Leskovšek, Wear Resistance and Anti-Sticking Properties of Duplex Treated Forming Tool Steel, *Wear*, Vol 254, 2003, p 1113–1121
61. B. Podgornik and S. Hogmark, Surface Modification to Improve Friction and Galling Properties of Forming Tools, *J. Mater. Process*., Vol 174, 2006, p 334–341
62. T. Klünsner, F. Zielbauer, S. Marsoner, M. Deller, M. Morstein, and C. Mitterer, Influence of Surface Topography on Early Stages on Steel Galling of Coated WC-Co Hard Metals, *Int. J. Refract. Met. Hard Mater*., Vol 57, 2016, p 24–30
63. J.L. Andreasen, N. Bay, and L. De Chiffre, Quantification of Galling in Sheet Metal Forming by Surface Topography Characterisation, *Int. J. Mach. Tools Manuf*., Vol 38, 1998, p 503–510
64. P. Karlsson, A. Gåård, P. Krakhmalev, and J. Bergström, Galling Resistance and Wear Mechanisms for Cold-Work Tool Steels in Lubricated Sliding against High Strength Stainless Steel Sheets, *Wear*, Vol 286–287, 2012, p 92–97
65. B. Voss, "Galling Wear Detection and Measurement in Sheet Metal Forming," Ph.D. thesis, Australian National University, Canberra, 2018
66. L. Pelcastre, J. Hardell, and B. Prakash, Galling Mechanisms during Interaction of Tool Steel and Al-Si Coated Ultra-High Strength Steel at Elevated Temperature, *Tribol. Int*., Vol 67, 2013, p 263–271
67. P. Karlsson, A. Gåård, and P. Krakhmalev, Influence of Tool Steel Microstructure on Friction and Initial Material Transfer, *Wear*, Vol 319, 2014, p 12–18
68. E. Schedin, Galling Mechanisms in Sheet Forming Operations, *Wear*, Vol 179, 1994, p 123–128
69. J. Heinrichs and S. Jacobson, Laboratory Test Simulation of Aluminium Cold Forming—Influence from PVD Tool Coatings on the Tendency to Galling, *Surf. Coat. Technol*., Vol 204, 2010, p 3606–3613
70. B. Podgornik, S. Hogmark, and O. Sandberg, Influence of Surface Roughness and Coating Type on the Galling Properties of Coated Forming Tool Steel, *Surf. Coat. Technol*., Vol 184, 2004, p 338–348
71. Y. Hou, Z. Yu, and S. Li, Galling Failure Analysis in Sheet Metal Forming Process, *J. Shanghai Jiaotong Univ. (Sci.)*, Vol 15, 2010, p 245–249
72. "Pin Wear from Galling," John King Group Co., https://www.johnkingchains.com/technical-data/analysis-of-damage-cause-and-remedies/21-4-pin-wear-from-galling/, accessed Jan 10, 2019
73. "Galling," Tribonet, https://www.tribonet.org/?s=galling, accessed Jan 10, 2019
74. L. Figueiredo, A. Ramalho, M.C. Oliveira, and L.F. Menezes, Experimental Study of Friction in Sheet Metal Forming, *Wear*, Vol 271, 2011, p 1651–1657
75. S.R. Hummel, Development of a Galling Resistance Test Method with a Uniform Stress Distribution, *Tribol. Int*., Vol 41, 2008, p 175–180
76. J.A. Siefert and S.S. Babu, Experimental Observations of Wear in Specimens Tested to ASTM G 98, *Wear*, Vol 320, 2014, p 111–119
77. "Standard Test Method for Galling Resistance of Materials," G 98, ASTM International, West Conshohocken, PA, 2009, http://dx.doi.org/10.1520/G0098-02R09
78. "Program on Technology Innovation: Galling and Sliding Wear Test Results for Candidate Hardfacing Alloys Manufactured by PM/HIP," EPRI, Palo Alto, CA, 3002001737, 2013
79. B.M. Voss, M.P. Pereira, B.F. Rolfe, and M.C. Doolan, A New Methodology for Measuring Galling Wear Severity in High Strength Steels, *Wear*, Vol 390–391, 2017, p 334–345
80. S.R. Hummel, An Application of Frictional Criteria for Determining Galling Thresholds Is Line Contact Tests, *Tribol. Int*., Vol 35, 2002, p 801–807
81. L.K. Ives, M.B. Peterson, and E.P. Whitenton, "The Mechanism, Measurement, and Influence of Properties on the Galling of Metals," NISTIR 89-4064, National Institute of Standards and Technology, Gaithersburg, MD, 1989
82. D.D. Olsson, N. Bay, and J.L. Andreasen, A Quantitative Lubricant Test for Deep Drawing, *Int. J. Surf. Sci. Eng*., Vol 4, 2010, p 2–12
83. S.R. Hummel, New Test Method and Apparatus for Measuring Galling Resistance, *Tribol. Int*., Vol 34, 2001, p 593–597
84. K.G. Budinski, M.K. Budinski, and M.S. Kohler, A Galling-Resistant Substitute for Silicon Nickel, *Wear*, Vol 255, 2003, p 489–497
85. S. Morris, R.J.K. Wood, T.J. Harvey, and H.E.G. Powrie, Use of Electrostatic Charge Monitoring for Early Detection of Adhesive Wear in Oil Lubricated Contacts, *J. Tribol*., Vol 124, 2002, p 288–296
86. O. Tasbaz, R. Wood, M. Browne, H. Powrie, and G. Denuault, Electrostatic Monitoring of Oil Lubricated Sliding Point Contacts for Early Detection of Scuffing, *Wear*, Vol 230, 1999, p 86–97
87. J. Han, R. Zhang, O. Ajayi, G. Barber, Q. Zou, L. Guessous, D. Schall, and S. Alnabulsi, Scuffing Behaviour of Gray Iron and 1080 Steel in Reciprocating and Rotational Sliding, *Wear*, Vol 271, 2011, p 1854–1861
88. P.A. Swanson, L.K. Ives, E.P. Whiteton, and M.B. Peterson, A Study of the Galling of Two Steels Using Two Test Methods, *Wear*, Vol 122, 1998, p 207–223
89. B. Podgornik, S. Hogmark, and J. Pezdirnik, Comparison between Different Test Methods for Evaluation of Galling Properties of Surface Engineered Tool Surfaces, *Wear*, Vol 257, 2004, p 843–851
90. T.J. Kamps, J.C. Walker, R.J. Wood, P. M. Lee, and A.G. Plint, Reproducing Automotive Engine Scuffing Using a

Lubricated Reciprocating Contact, *Wear*, Vol 332–333, 2015, p 1193–1199
91. M. Ingram, C. Hamer, and H. Spikes, A New Scuffing Test Using Contra-Rotation, *Wear*, Vol 328–329, 2015, p 229–240
92. H. Blok, Gear Wear as Related to Viscosity of Gear Oils, *Proc. Summer Conf.—MIT, Mech. Wear*, Vol 61 (No. 25), ASME, June 1948, p 199–227
93. L.V. Wedeven, Method and Apparatus for Comprehensive Evaluation of Tribological Materials, U.S. Patent 5,679,883, 1997
94. L.M. Bernick, R.R. Hilsen, and C.L. Wandrei, Development of a Quantitative Sheet Galling Test, *Wear*, Vol 48 (No. 2), 1978, p 323–346
95. E. Üstünyagiza, C.V. Nielsen, and P. Christiansen, Continuous Strip Reduction Test Simulating Tribological Conditions in Ironing, *Proc. Eng*., Vol 207, 2017, p 2286–2291
96. M. Hirasaka and H. Nishimura, Effects of the Surface Micro-Geometry of Steel Sheets on Galling Behaviour, *J. Mater. Process. Technol*., Vol 47, 1994, p 153–166
97. E. Heidevan der, A.J. Huis in't Veld, and D.J. Schipper, The Effect of Lubricant Selection on Galling in a Model Wear Test, *Wear*, Vol 251, 2001, p 973–979
98. M. Söderfjäll, A. Almqvist, and R. Larsson, Component Test for Simulation of Piston Ring-Cylinder Liner Friction at Realistic Speeds, *Tribol. Int*., Vol 104, 2016, p 57–63
99. H.M. Herbst and H.H. Priebsch, Simulation of Piston Ring Dynamics and Their Effect on Oil Consumption, *SAE Trans*., *J. Eng*., Vol 109 (No. 3), 2000, p 862–873
100. S. Hogmark, S. Jacobson, and O. Wanstrand, A New Universal Test for Tribological Evaluation, *Proc. 22nd Meeting of the International Research Group on Wear of Engineering Materials (IRG-OECD)*, University of Cambridge, U.K., Sept 2000
101. "Machining, Forming and Forging Tests," http://www.phoenix-tribology.com/wp-content/uploads/guidance/Guidance-Machining-Forming-Forging-Tests.pdf,
102. A. Ramalho, Study of the Relationships Friction-Contact Stresses Using Load Scanner Tests, *Proc. Eleventh Nordic Symposium on Tribology (NORDTRIB2004)*, 2004, p 699–707
103. D.H.E. Persson, S. Jacobson, and S. Hogmark, Effect of Temperature on Friction and Galling of Laser Processed Norem 02 and Stellite, *Wear*, Vol 255, 2003, p 498–503
104. U. Wilkund and I.M. Hutchings, Investigation of Surface Treatments for Galling Protection of Titanium Alloys, *Wear*, Vol 251, 2001, p 1034–1041
105. V.V. Shanbhag, B.F. Rolfe, J.M. Griffin, N. Arunachalam, and M.P. Pereir, Understanding Galling Wear Initiation and Progression Using Force and Acoustic Emissions Sensors, *Wear*, Vol 436–437, 2019, p 202991
106. M. Tisza and T. Fülöp, A General Overview of Tribology of Sheet Metal Forming, *J. Technol. Plast*., Vol 2, 2001, p 11–25
107. B.H. Lee, Y.T. Keum, and R.H. Wagoner, Modeling of the Friction Caused by Lubrication and Surface Roughness in Sheet Metal Forming, *J. Mater. Process. Technol*., Vol 130–131, 2002, p 60–63
108. J.H.C. Souzade and M. Liewald, Analysis of the Tribological Behaviour of Polymer Composite Tool Materials for Sheet Metal Forming, *Wear*, Vol 268, 2010, p 241–248
109. V. Severo, L. Vilhena, P.N. Silva, J.P. Dias, D. Becker, S. Wagner, and A. Cavaleiro, Tribological Behaviour of W-Ti-N Coatings in Semi-Industrial Strip-Drawing Tests, *J. Mater. Process. Technol*., Vol 209–210, 2009, p 4662–4667
110. H. Kim, J.H. Sung, R. Sivakumar, and T. Altan, Evaluation of Stamping Lubricants Using the Deep Drawing Test, *Int. J. Mach. Tool Manuf*., Vol 47, 2007, p 2120–2132
111. H. Gong, Z. Lou, and Z. Zhang, Studies on the Friction and Lubrication Characteristics in the Sheet Steel Drawing Process, *J. Mater. Process. Technol*., Vol 151, 2004, p 328–333
112. H.Y. Kim, B.C. Whang, and W.B. Bae, An Experimental Study on Forming Characteristics of Pre-Coated Sheet Steels, *J. Mater. Process. Technol*., Vol 120, 2002, p 290–292
113. S.S. Han, The Influence of Tool Geometry on Friction Behaviour in Sheet Metal Forming, *J. Mater. Process. Technol*., Vol 63, 1997, p 129–133
114. M.R. Lovell and Z. Deng, Characterization of Interfacial Friction in Coated Sheet Steels: Influence of Stamping Process Parameters and Wear Mechanisms, *Tribol. Int*., Vol 35, 2002, p 85–95
115. M. Samuel, Influence of Drawbead Geometry on Sheet Metal Forming, *J. Mater. Process. Technol*., Vol 122, 2002, p 94–103
116. H.D. Nine, *Draw Bead Forces in Sheet Metal Forming*, *Proceedings of a Symposium on Mechanics of Sheet Metal Forming: Behaviour and Deformation Analysis* (Warren, MI), Plenum Press, 1978, p 179–211
117. L.R. Sanchez, Characterisation of a Measurement System for Reproducible Friction Testing on Sheet Metal under Plane Strain, *Tribol. Int*., Vol 32, 1999, p 575–586
118. J.L. Duncan, B.S. Shabel, and J.G. Filho, "*A Tensile Strip Test for Evaluating Friction in Sheet Metal Forming*," SAE Technical Paper 780391, 1978
119. K. Seshacharyulu, C. Bandhavi, B. Balu Naik, S.S. Rao, and S.K. Singh, Understanding Friction in Sheet Metal Forming—A Review, *Mater. Today: Proc*., Vol 5, 2018, p 18238–18244
120. C.T. Sindi, M.A. Najafabadi, and M. Salehi, Tribological Behaviour of Sheet Metal Forming Process Using Acoustic Emission Characteristics, *Tribol. Lett*., Vol 52, 2013, p 6–9
121. S. Mostafavi, C.T. Sindi, F. Pashmforoush, and R.F. Zinati, Acoustic Emission Waves from the Onset of Galling between Tool and Sheet Material, *Mater. Eval*., Vol 71, 2013, p 1335–1342
122. M. Moghadam, P. Christiansen, and N. Bay, Detection of the Onset of Galling in Strip Reduction Testing Using Acoustic Emission, *Proc. Eng*., Vol 183, 2017, p 59–64
123. H. Czichos and K. Kirschke, Investigation into Film Failure (Transition Point) of Lubricated Concentrated Contacts, *Wear*, Vol 22 (No. 3), 1972, p 321–336
124. J. Qu, J.J. Truhan, and P.J. Blau, Investigation of the Scuffing Characteristics of Candidate Materials for Heavy Duty Diesel Fuel Injectors, *Tribol. Int*., Vol 38, 2005, p 381–390
125. P.J. Blau, M. Yao, J. Qu, and J. Wu, Use of Multiple Criteria to Map the High-Temperature Scuffing Behaviour of Co-Based Super Alloys, *Wear*, Vol 267, 2009, p 374–379
126. H. Yoon, J. Zhang, and F. Kelley, Scuffing Characteristics of SAE 50B38 Steel under Lubricated Conditions, *Tribol. Trans*., Vol 45 (No. 2), 2002, p 246–252
127. R.W. Snidle, A.K. Dhulipalla, H.P. Evans, and C.V. Cooper, Scuffing Performance of a Hard Coating under EHL Conditions at Sliding Speeds up to 16 m/s and Contact Pressures up to 2.0 GPa, *J. Tribol*., Vol 130 (No. 2), 2008, p 021301
128. M.J. Patching, C.C. Kweh, H. Evans, and R.W. Snidle, Conditions for Scuffing Failure of Ground and Superfinished Steel Disks at High Sliding Speeds Using a Gas Turbine Engine Oil, *J. Tribol*., Vol 117, 1995, p 482–489
129. J. Kleemola and A. Lehtovaara, An Approach for Determination of Lubricant Properties at Elliptical Elastohydrodynamic Contacts Using a Twin-Disc Test Device and a Numerical Traction Model, *Proc. Inst. Mech. Eng*., Vol 222, 2008, p 797–806
130. V. Simon, Load Distribution in Spiral Bevel Gears, *ASME J. Mech. Des*., Vol 129, 2006, p 201–209
131. C. Gorla, F. Rosa, E. Conrado, and H. Albertini, Bending and Contact Fatigue Strength of Innovative Steels for Large Gears, *Proc. Inst. Mech. Eng. C, J. Mech. Eng. Sci*., Vol 228 (No. 14), 2014, p 2469–2482

132. O.O. Ajayi, M.F. Alzoubi, A. Erdemir, and G.R. Fenske, Effect of Carbon Coating on Scuffing Performance in Diesel Fuels, *Tribol. Trans.*, Vol 44 (No. 2), 2001, p 298–304
133. P. Olander, S.S. Eskildsen, J.W. Fogh, P. Hollman, and S. Jacobson, Testing Scuffing Resistance of Materials for Marine 2-Stroke Engines—Difficulties with Lab Scale Testing of a Complex Phenomenon, *Wear*, Vol 340–341, 2015, p 9–18
134. J. Qu, J.J. Truhan, P.J. Blau, and H.M. Meyer III, Scuffing Transition Diagrams for Heavy Duty Diesel Fuel Injector Materials in Ultra Low-Sulfur Fuel-Lubricated Environment, *Wear*, Vol 259, 2005, p 1031–1040
135. B.-R. Höhn, K. Michaelis, and H.-P. Otto, Pitting Load Carrying Capacity under Increased Thermal Conditions, *Third International Conference on Integrity, Reliability and Failure*, July 20–24, 2009 (Porto, Portugal), p 1–10
136. J. Castro, A. Sottomayor, and J. Seabra, Experimental and Analytical Scuffing Criteria for FZG Gears, *Transient Processes in Tribology,* G. Dalmaz et al., Ed., Vol 43, 2003, p 651–661
137. H. Winter and K. Michaelis, FZG Gear Test Rig—Description and Test Possibilities, *Co-Ordinate European Council Second International Symposium on the Performance Evaluation of Automotive Fuels and Lubricants* (Wolfsburg, West Germany), 1985, p 29–42
138. J. Castro and J. Seabra, Global and Local Analysis of Gear Scuffing Tests Using a Mixed Film Lubrication Model, *Tribol. Int.*, Vol 41, 2008, p 244–255
139. J. Castro and J. Seabra, Scuffing and Lubricant Film Breakdown in FZG Gears, Part I: Analytical and Experimental Approach, *Wear*, Vol 215, 1998, p 104–113
140. J. Castro and J. Seabra, Scuffing and Lubricant Film Breakdown in FZG Gears, Part II: New PV Scuffing Criteria, Lubricant and Temperature Dependent, *Wear*, Vol 215, 1998, p 114–122
141. K. Michaelis, B.-R. Höhn, and P. Oster, Influence of Lubricant on Gear Failures—Test Methods and Application to Gear Boxes in Practice, *Tribotest J.*, Vol 11 (No. 1), 2004, p 43–56
142. W. Tuszynski, R. Michalczewski, M. Szczerek, and M. Kalbarczyk, A New Scuffing Shock Test Method for the Determination of the Resistance to Scuffing of Coated Gears, *Arch. Civil Mech. Eng.*, Vol 12, 2012, p 436–445
143. W. Tuszynski, M. Kalbarczyk, M. Michalak, R. Michalczewski, and A. Wieczorek, The Effect of WC/C Coating on the Wear of Bevel Gears Used in Coal Mines, *Mater. Sci. Medzg.*, Vol 21 (No. 8), 2015, p 358–363
144. E. Conrado, B.-R. Höh, K. Michaelis, and M. Klein, Influence of Oil Supply on the Scuffing Load-Carrying Capacity of Hypoid Gears, *Proc. Inst. Mech. Eng.*, Vol 221, 2007, p 851–858
145. P. Obert, T. Müller, H.-J. Füßer, and D. Bartel, The Influence of Oil Supply and Cylinder Liner Temperature on Friction, Wear and Scuffing Behaviour of Piston Ring Cylinder Liner Contacts—A New Model Test, *Tribol. Int.*, Vol 94, 2016, p 306–314
146. P. Karlsson, P. Krakhmalev, A. Gåård, and J. Bergström, Influence of Work Material Proof Stress and Tool Steel Microstructure on Galling Initiation and Critical Contact Pressure, *Tribol. Int.*, Vol 60, 2013, p 104–110
147. G.A. Fontalvo, R. Humer, C. Mitterer, K. Sammt, and I. Schemmel, Microstructural Aspects Determining the Adhesive Wear of Tool Steels, *Wear*, Vol 260, 2006, p 1028–1034
148. A. Gåård, P. Krakhmalev, J. Bergström, and N. Hallbäck, Galling Resistance and Wear Mechanisms—Cold Work Tool Materials Sliding against Carbon Steel Sheets, *Tribol. Lett.*, Vol 26, 2006, p 67–72
149. A. Gåård, P. Krakhmalev, and J. Bergström, Wear Mechanisms in Galling: Cold Work Tool Materials Sliding against High-Strength Carbon Steel Sheets, *Tribol. Lett.*, Vol 33, 2009, p 45–53
150. I. Heikkilä, L. Slycke, and O. Sandberg, Influence of Nitrogen Alloying on Galling Properties of PM Tool Steels, *Proceedings of the Sixth International Tooling Conference*, J. Bergström, Ed., Karlstad University Press, Karlstad, 2002, p 217–226
151. O. Sandberg, Advanced Low Friction Tool Steel for Metal Processing—Properties and Industrial Experiences, *Proceedings of the Seventh International Tooling Conference*, M. Rosso, Ed., Politecnico di Torino, Turin, 2006, p 13–20
152. I. Heikkilä, M. Lundberg, L. Gunnarsson, A. Feiler, and M. Rutland, The Contribution of the Surface Properties of Tool Steels for Galling Behaviour in Sheet Metal Forming, *Proceedings of the Seventh International Tooling Conference*, M. Rosso, Ed., Politecnico di Torino, Turin, 2006, p 351–358
153. S. Hatami, A. Nafari, L. Nyborg, and U. Jelvestam, Galling Related Surface Properties of Powder Metallurgical Tool Steels Alloyed with and without Nitrogen, *Wear*, Vol 269, 2010, p 229–240
154. P. Groche, M. Christiany, and Y. Wu, Load-Dependent Wear in Sheet Metal Forming, *Wear*, Vol 422–23, 2019, p 252–260
155. *Review of the Wear and Galling Characteristics of Stainless Steels*, Committee of Stainless Steel Producers, American Iron and Steel Institute, Washington, D.C., 1978
156. W.J. Schumacher, Wear and Galling Can Knock out Equipment, *Chem. Eng.*, 1977, p 155–160
157. S. Hummel and B. Partlow, Threshold Galling Load and Frictional Behaviour of Stainless Steel in Line Contact, *Wear*, Vol 255, 2003, p 504–508
158. W.J. Schumacher, New Galling Data Aid in Selecting Stainless Steel, *Mater. Eng.*, Vol 4, 1973, p 61–63
159. W.J. Schumacher, *Adhesive Wear of Engineering Alloys*, *Met. Prog.,* Nov 1978, p 32–36
160. I. Hekkilä, Influence of Tool Steel Microstructure on Galling Resistance against Stainless Steel, *Proc. of the 30th Leeds-Lyon Symposium on Tribology*, D. Dowson et al., Ed., INSA de Lyon Villebanne, France, 2003, p 641–650
161. F.P. Fehlner and N.F. Mott, Low Temperature Oxidation, *Oxid. Met.*, Vol 2, 1970, p 59–99
162. T. Arai and Y. Tsuchiya, Role of Carbides and Nitrides in Anti-Galling Property of Die Materials and Surface Coatings, *Metal Transfer and Galling in Metallic Systems*, H.D. Merchant and K. J. Bhansali, Ed., The Metallurgical Society, Warrendale, PA, 1986, p 197–216
163. B. Podgornik, J. Vizintin, and S. Hogmark, Improvement in Galling Performance through Surface Engineering, *Surf. Eng.*, Vol 22, 2006, p 235–238
164. M. Savolainen and A. Lehtovaara, An Experimental Investigation of Scuffing Initiation due to Axial Displacement in a Rolling/Sliding Contact, *Tribol. Int.*, Vol 119, 2018, p 688–697
165. S. Wan, D. Li, G. Zhang, A.K. Tieu, and B. Zhang, Comparison of the Scuffing Behaviour and Wear Resistance of Candidate Engineered Coatings for Automotive Piston Rings, *Tribol. Int.*, Vol 106, 2017, p 10–22
166. A. Erdemir and C. Donnet, Tribology of Diamond-Like Carbon Films: Recent Progress and Future Prospects, *J. Phys. D, Appl. Phys.*, Vol 39, 2006, p R311–R327
167. B. Podgornik, S. Hogmark, and O. Sandberg, Proper Coating Selection for Improved Galling Performance of Forming Tool Steel, *Wear*, Vol 261, 2006, p 15–21
168. B. Podgornik, V. Leskovšek, and J. Vizintin, Influence of Deep-Cryogenic Treatment on Tribological Properties of P/M High-Speed Steel, *Mater. Manuf. Process.*, Vol 24, 2009, p 734–738
169. S. Saketi, J. Östby, and M. Olsson, Influence of Tool Surface Topography on the Material Transfer Tendency and Tool Wear in the Turning of 316L Stainless Steel, *Wear*, Vol 368–369, 2016, p 239–252
170. O. Mahrenholz, N. Botcheva, and R. Iankov, Influence of Surface Roughness on Friction during Metal Forming Processes, *J. Mater. Process. Technol.*, Vol 159, 2005, p 9–16

171. M. Hanson, S. Hogmark, and S. Jacobson, Influence from Tool Roughness on the Risk of Work Material Adhesion and Transfer, *Mater. Manuf. Process.*, Vol 24, 2009, p 913–917
172. V. Westlund, J. Heinrichs, M. Olsson, and S. Jacobson, Investigation of Material Transfer in Sliding Friction—Topography or Surface Chemistry? *Tribol. Int.*, Vol 100, 2016, p 213–223
173. M. Sedlaček, B. Podgornik, and J. Vizintin, Correlation between Standard Roughness Parameters Skewness and Kurtosis and Tribological Behaviour of Contact Surfaces, *Tribol. Int.*, Vol 48, 2012, p 102–112
174. I. Etsion, G. Halperin, and E. Becker, The Effect of Various Surface Treatments on Piston Pin Scuffing Resistance, *Wear*, Vol 261, 2006, p 785–791
175. B. Podgornik, L.M. Vilhena, M. Sedlaček, Z. Rek, and I. Žun, Effectiveness and Design of Surface Texturing for Different Lubrication Regimes, *Meccanica*, Vol 47, 2012, p 1613–1622
176. F.P. Bowden and D. Tabor, *The Friction and Lubrication of Solids, Part 2*, Oxford University Press, 1964
177. E. Rabinowicz, The Influence of Compatibility on Different Tribological Phenomena, *ASLE Trans.*, Vol 14, 1971, p 206–212
178. D.H. Buckley and K. Miyoshi, Friction and Wear of Ceramics, *Wear*, Vol 100, 1984, p 333–353
179. E. Lugscheider and K. Bobzin, The Influence on Surface Free Energy of PVD-Coatings, *Surf. Coat. Technol.*, Vol 142–144, 2001, p 755–760